# PETROFABRIC ANALYSIS OF EXPERIMENTALLY DEFORMED CALCITE-CEMENTED SANDSTONES

M. FRIEDMAN

Reprinted for private circulation from
THE JOURNAL OF GEOLOGY
Vol. 71, No. 1, January 1963

# PETROFABRIC ANALYSIS OF EXPERIMENTALLY DEFORMED CALCITE-CEMENTED SANDSTONES[1]

M. FRIEDMAN[2]

ABSTRACT

Cylinders of sand crystals, composed of single crystals of calcite that poikilitically enclose detrital grains, and calcite-cemented sandstones from the Tensleep (Pennsylvanian, Wyoming) and Supai (Permian, Nevada) formations were experimentally deformed dry at confining pressures of 1–5 kilobars and temperatures of 150°–300° C. Thin sections of the undeformed and deformed specimens were studied microscopically to gain a better understanding of the behavior of sandstones in simulated tectonic environments. The calcite and the detrital grains (quartz, feldspar, and others), which have radically different physical and mechanical properties, are shown statistically to have deformed with respect to the principal stresses across the boundaries of the whole specimens rather than with regard to local stress concentrations at grain contacts.

The deformation mechanisms of calcite and quartz are the same in the sandstones as in monomineralic aggregates, such as marbles and quartz sands. Statistically, twin lamellae are developed in those calcite grains that are favorably oriented for twin gliding with respect to the load axes. The resolved shear-stress coefficient for these twin planes averages 0.27. Compression and extension axes deduced from the best developed set of twin lamellae in each calcite grain yield derived positions for the principal stress axes that are in excellent agreement with those known from the experiments. In addition, the number of lamellae per millimeter increases with increased strain of the specimens.

Quartz, feldspar, rock fragments, and garnet grains comprise the bulk of the detrital material. These deform primarily by fracturing. The microfractures in the grains are nearly planar features which, because of their geometric relationship to the known principal stress directions, are recognized as extension and shear fractures. They develop independently of the grain mineralogy and, in quartz grains, greatly overshadow a slight tendency for fractures to parallel $r\{10\bar{1}1\}$ and $z\{01\bar{1}1\}$. The degree of fracturing in a specimen, expressed as a fracture index, tends to increase with increased strain of the specimen. In sand crystals loaded unfavorably for twin gliding in the calcite crystal, extension fracturing in the detrital grains causes local reorientation of the stresses and produces twin lamellae in the adjacent calcite.

Twin lamellae in calcite and fractures in detrital grains are shown to be criteria for simulated tectonism. The development of lamellae and microfractures is directly related to the orientations of the principal stresses in heterogeneous, sedimentary rocks at the time of deformation.

## INTRODUCTION

Structural configurations are dependent upon stress conditions in rocks during tectonic events. This has been demonstrated theoretically by the treatments of Anderson (1951), Hafner (1951), Hubbert (1951), Odé (1957), Hubbert and Rubey (1959), and Sanford (1959), to name a few. Moreover, the fact that the behavior of rocks with respect to states of stress and other tectonic environmental factors can be predicted has been experimentally demonstrated primarily by the studies of Griggs and of Handin and their associates.[3] Until recently, however, it has not been possible to augment these treatments by direct determination of the principal stress orientations in rocks at the time of deformation. Petrofabric techniques, based upon detailed knowledge of the mechanisms of deformation in a number of commonly occurring minerals, now permit such determinations. Some of these techniques have been applied successfully to the study of monomineralic, metamorphic rocks (Turner, 1953; McIntyre and Turner, 1953; Gilmour and Carman, 1954; Weiss, 1954; Crampton, 1958; and Christie, 1958).

The present study was designed to evaluate twin lamellae in calcite and fractures in detrital grains as sound criteria of deformation in deformed, heterogeneous, sedi-

[1] Publication No. 251, Shell Development Company (A Division of Shell Oil Company), Exploration and Production Research Division, Houston, Texas. Manuscript received August 10, 1961.

[2] Geologist, Shell Development Company, Houston, Texas.

[3] See Griggs (1936, 1939); Griggs and Bell (1938); Griggs and Miller (1951); Griggs, Turner, Borg, and Sosoka (1951, 1953); Griggs and Handin (1960); and Griggs, Turner, and Heard (1960); Handin and Griggs (1951); Handin (1953); Handin and Fairbairn (1955); and Handin and Hager (1957, 1958).

mentary rocks. If these microfeatures constitute a deformation record and can be used to obtain a stress pattern, a potentially valuable technique would be added to the tools of petrofabric analysis. It must be demonstrated, however, that these features are meaningful—that in a heterogeneous, porous aggregate the individual mineral components react relative to the principal stresses across the boundaries of the rock as a whole rather than a local stress concentrations at grain contacts. Accordingly, experimentally deformed sand crystals and calcite-cemented sandstones were studied to evaluate the significance of the microfeatures in the calcite and quartz of these materials for which the stress situations across the boundaries of the specimens are known.

## Previous Work

The study is based upon the relationships between the three principal compressive stresses (greatest, $\sigma_1$; intermediate, $\sigma_2$; and least, $\sigma_3$) and (1) twin gliding in calcite and (2) fractures in detrital grains such as quartz, feldspars, and rock fragments.

### CALCITE

Knowledge of the deformation mechanisms in calcite has evolved from Brewster's observatious of mechanical twins in 1826 to the comprehensive experimental studies of deformed calcite single crystals and marbles and the petrofabric analysis of the deformed materials (Knopf, 1949; Turner, 1949; Griggs and Miller, 1951; Handin and Griggs, 1951; Turner and Ch'ih, 1951; Griggs, Turner, Borg, and Sosoka, 1951, 1953; Borg and Turner, 1953; Turner, Griggs, and Heard, 1954; Turner, Griggs, Clark, and Dixon, 1956; Griggs, Turner, and Heard, 1960). As a result, flow in calcite can be primarily explained by three glide systems (fig. 1):

1. Twin gliding parallel to $e\ \{01\bar{1}2\}$ with $[e_1:r_2]$ as the glide direction, and with a positive sense of shear.[4] This mechanism is effective throughout the temperature range of 20°–800° C.

2. Translation gliding on $r\{10\bar{1}1\}$ with $[r_1:f_2]$ as the glide direction, sense of shear negative. It is effective over the temperature range 20°–800° C.[5]

3. Translation gliding on $f\{02\bar{2}1\}$ with $[f_1:r_3]$ as the glide direction, sense of shear negative. It is effective at 20° C. and at 500°–800° C., and in the latter temperature range it predominates over $r$ translation.

Twin gliding[6] is dependent upon a critical resolved shear stress ($\tau_c$) on the twin plane but is essentially independent of normal stress across the twin plane (Turner, Griggs, and Heard, 1954, p. 889). Turner and Ch'ih (1951, p. 899–900) amply demonstrated for experimentally deformed Yule marble that the greatest amount of twinning occurs on that $e$-plane (designated $e_1$) on which the shear stress, or the resolved shear-stress coefficient ($S_0$),[7] is highest. Turner (1953) made a dynamic interpretation of twin lamellae in naturally deformed marbles by employing the petrofabric technique of locating the mutually perpendicular directions of compression and extension that most favored development of the observed twin lamellae. The geometry of these relationships was initially set forth by Handin and Griggs (1951, p. 866–869). If a maximum $S_0$ value (0.5) for twinning is assumed, the position of the load axis can be uniquely defined, because both $\chi_0$ and $\lambda_0$ must be 45°. Accordingly, $\sigma_1'$ and $\sigma_3'$[8] are fixed for twin gliding when $S_0 = 0.5$ (fig. 2, $a$); $\sigma_1'$ (com-

[4] Arbitrarily, relative displacement of the upper layers of the lattice upward toward the optic axis ($c_V$) is called gliding in the positive sense; relative displacement of the upper layers downward from the upper end of the $c_V$ is called gliding in the negative sense.

[5] Translation gliding does not result in reorientation of the crystal structure as in twin gliding. Moreover, visible evidence of translation (such as slip lines) is rare. Because of this, translation gliding systems were not utilized in this study.

[6] For a more detailed treatment of the twinning process see Bell (1941), Hall (1954), Pabst (1955), and Higgs and Handin (1959), among others.

[7] $S_0 = \sin \chi_0 \cos \lambda_0$ where $\chi_0$ = angle between load axis and glide plane and $\lambda_0$ = angle between load axis and glide line.

[8] Primes are used to denote derived principal stress axes.

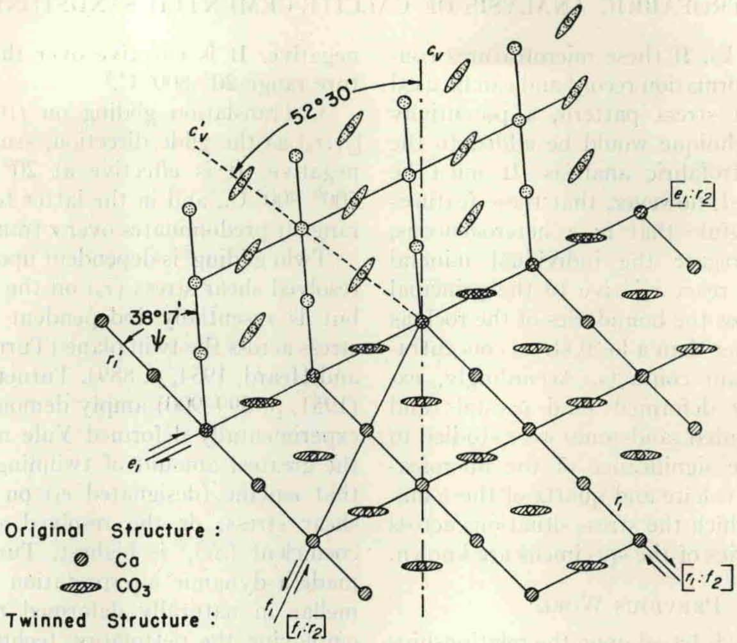


FIG. 1.—Diagrammatic representation of section through calcite structure. Section is drawn normal to $a_2$ axis, i.e., plane of section is normal to twin plane $e_1$ and contains glide line $[e_1:r_2]$. Structure is twinned on $e_1$ plane, with glide direction and sense of shear indicated. $r_1$ and $f_1$ translation glide planes, glide directions, and senses of shear are also indicated.

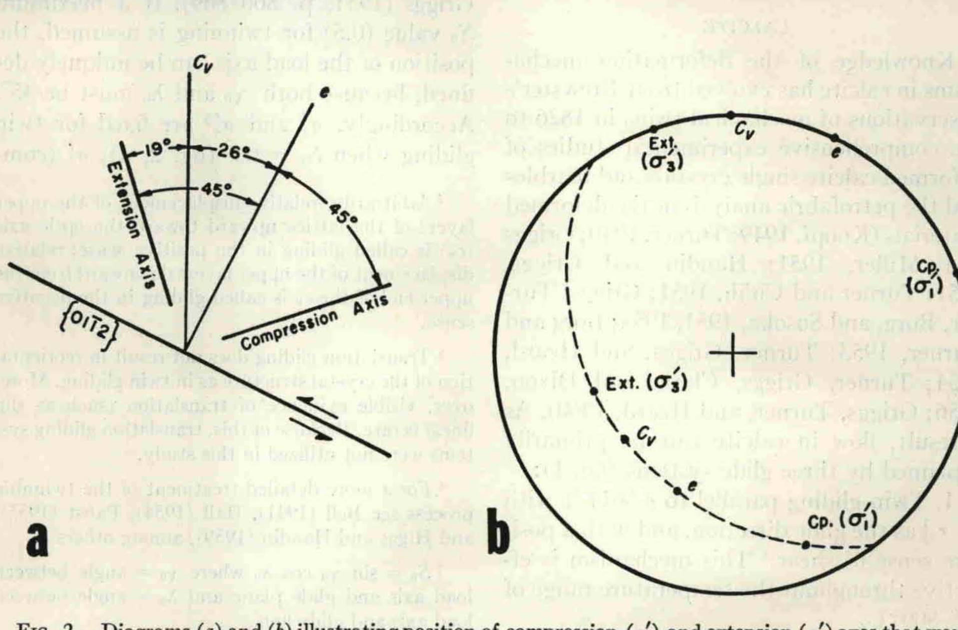


FIG. 2.—Diagrams (*a*) and (*b*) illustrating position of compression ($\sigma'_1$) and extension ($\sigma'_3$) axes that would be most effective in causing observed *e* twin lamellae in a calcite crystal. Section is normal to *e* plane and contains glide direction and optic axis ($c_V$).

pression axis) is inclined 45° to $e_1$,[9] or to the normal to $e_1$, and 71° to $c_v$; and $\sigma_3'$ (extension axis) is inclined 45° to $e_1$, or to the normal to $e_1$, and 19° to $c_v$. For any calcite grain, therefore, the positions of $\sigma_1'$ and $\sigma_3'$ for $S_0 = 0.5$ can be determined (fig. 2, *b*) by measuring and plotting $e_1$ and $c_v$. This technique was applied to the study of naturally deformed marbles by Turner (1953), McIntyre and Turner (1953), Gilmour and Carman (1954), and Weiss (1954). These workers concluded that the calcite twin lamellae developed during the last stages of deformation. Crampton (1958) and Christie (1958) extended the technique to deformed dolomites utilizing the information on the glide mechanisms in dolomite determined by Handin and Fairbairn (1955), Turner, Griggs, Heard, and Weiss (1954), and Higgs and Handin (1959). Hansen *et al.* (1959) studied deformed calcite cement in three oriented specimens of folded Oriskany sandstone. They found that the compression axes deduced from the best-developed sets of *e* twin lamellae were grouped essentially normal to the fold axis. This is the first published account of the use of this technique on a sedimentary rock.

FRACTURE

Many theoretical and experimental studies on fracturing are available dating from the early work of Coulomb (1776) to the current experimental studies of Handin and of Griggs. The following discussion pertains to microfractures[10] as well. Two kinds of fracture (extension and shear) are recognized (Griggs and Handin, 1960), and each bears consistent geometric relationships to the three principal stresses (fig. 3). Extension fracture is characterized by displacement normal to the fracture surface at the time of formation, and is oriented parallel to $\sigma_1$ and $\sigma_2$ and perpendicular to $\sigma_3$, as shown in figure 3, *A*. Shear fracture is characterized by shearing displacement along the fracture surface at the time of formation, and is inclined in rocks approximately 30° to $\sigma_1$ and 60° to $\sigma_3$, and is parallel to $\sigma_2$, as shown in figure 3, *B*. Theoretically, two sets of shear fractures form a conjugate system, with an included angle of approximately 60° which is bisected by $\sigma_1$. The angle between a shear

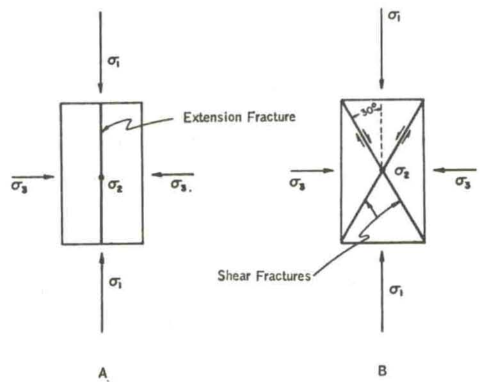


FIG. 3.—Orientation of fractures with respect to principal stress directions. *A*, extension fracture; *B*, shear fractures.

fracture and $\sigma_1$ varies within narrow limits. Handin and Hager (1957, 1958) show that in seventy compression experiments this angle ranges from 25° to 35° in two-thirds of the cases and from 20° to 40° in nearly all the cases. Although no completely satisfactory theory of rock fracture has been found up to the present time, the Coulomb-Mohr, or "internal-friction," theory best predicts the empirical results. Accordingly, from both theoretical and experimental considerations, the genetic relationships between the types of fractures and the principal stresses are known qualitatively.

QUARTZ-DETRITAL GRAINS

Previous studies of the deformation of sand and sandstones have dealt primarily

[9] By convention the three twin planes in each calcite crystal are designated as $e_1$, $e_2$, and $e_3$; $e_1$ is identified as the plane of highest spacing index and/or widest-developed lamellae, and $e_3$ is identified as the plane of lowest spacing index and/or least-developed lamellae. In a calcite crystal in which at least one set of twin lamellae is developed ($e_1$), the positions of the other two potential sets can be determined.

[10] The term "microfracture" is used to denote a fracture or fault within an individual detrital grain. The scale of the feature is determined by the grain size.

with quartz-rich aggregates. Work on the other common detrital elements as such is lacking. Data on the strength of quartz is reviewed in detail in Griggs, Turner, and Heard (1960, p. 67, fig. 12) and in Borg, Friedman, Handin, and Higgs (1960, p. 181). What is generally important here is that the strength even of unconfined quartz is enormous. The fact that grains in quartz aggregates can be broken under relatively small loads applied to the aggregate as a whole implies great stress concentrations in the individual grains.

Fracturing is the most conspicuous deformation mechanism in quartz detrital grains.[11] Griggs and Bell (1938), Fairbairn (1939), Ingerson and Ramisch (1942), Anderson (1945), Rowland (1946), Borg and Maxwell (1956), Bloss (1957), and Borg, Friedman, Handin, and Higgs (1960) have described fractures in a variety of quartz occurrences in both experimentally and naturally deformed environments. Their data indicate a tendency of quartz to fracture primarily parallel to $r\{10\bar{1}1\}$, $z\{01\bar{1}1\}$, $c\{0001\}$, $m\{10\bar{1}0\}$, and $a\{11\bar{2}0\}$. Recently, Christie, Heard, and LaMori (1960) have experimentally deformed single quartz crystals at 25 kilobars confining pressure in a bismuth medium and at room temperature. The crystals failed by faulting parallel to $c\{0001\}$, $r\{10\bar{1}1\}$, $z\{01\bar{1}1\}$, and rarely parallel to $m\{10\bar{1}0\}$ and $a\{11\bar{2}0\}$, respectively, even though these planes were not necessarily oriented favorably for shear fracturing. In experimentally deformed loose, dry sand aggregates. Borg and Maxwell (1956, p. 77) found that (1) the microfractures radiate from grain contacts, (2) the quartz tends to fracture primarily parallel to $r$ and $z$, and (3) the microfractures tend to lie approximately 15° to the known position of $\sigma_1$. In a study of deformed St. Peter sand aggregates, Borg, Friedman, Handin, and Higgs (1960, p. 165–181) also found that quartz has a certain tendency to fracture parallel to $r$ and $z$. More important, they demonstrated that the microfracture orientation patterns are nearly random in undeformed samples and in specimens subjected to uniform confining pressure only. In compression and extension experiments, however, the microfracture patterns exhibit a definite relationship to the principal stresses across the boundaries of the specimens and indicate that both shear- and extension-type fractures had formed. Bonham (1957) has made a descriptive study of microfractures in the quartz grains of the Miocene and Pliocene sandstones in the Pico anticline, Los Angeles County, California. He found that microfracture maxima correlate well with other geometric features of the anticlinal structure.

The evidence to date indicates that fracture in quartz tends to be controlled by two factors: (1) the crystal structure and (2) the orientation of the principal stresses across the boundaries of the specimens. In most of the experiments and studies mentioned above it is difficult to evaluate which of these factors is the more important. Certainly, the latest experiments of Christie, Heard, and LaMori (1960) conclusively demonstrate that the quartz structure controls the fracturing in deformed single crystals. Yet it has been a moot question which factor is more important in the quartz-sand aggregate. The present study adds to the understanding of this problem.

## Methods of Study

### OPTICAL MEASUREMENTS AND PLOTTING OF DATA

All measurements are made with the aid of a petrographic microscope equipped with a Zeiss-Winkel universal stage and object traverser. The probable error in locating $c_v$ by optical means is $\pm 2°$. Lamellae and microfractures can be located to within 1° when they are inclined to the plane of the section at angles greater than 70°. For inclinations of 30°–70°, the error may be $\pm 2°$. The total probable error in the position of any fabric element with respect to the known load axes is due to (1) fabrication of

[11] Other mechanisms of deformation that give rise to, e.g., undulatory extinction and deformation lamellae are not discussed here because these features were not produced in the deformed specimens of the current study.

the original rock cylinder and end cups, (2) preparation of the oriented thin section, (3) optical measurements, and (4) plotting. The error may be as much as 10°, but it rarely exceeds 5°.

Thin sections from sand-crystal specimens are cut parallel to the long axis of each deformed cylinder. Thin sections from calcite-cemented sandstone specimens are cut both parallel and normal to the axis of each cylinder.

The point-count method (Chayes, 1956) is used to obtain modal analyses of experimentally deformed materials. "Point" spacing is 100 $\mu$, and data are recorded for six hundred points per specimen.

All measured data (orientation of $c_v$, calcite twin lamellae, and microfracture surfaces in quartz and in other detrital grains) and the derived positions of compression and extension axes are plotted stereographically on a Lambert-Schmidt equal-area net. The lower hemisphere of the projection sphere is projected on the horizontal plane.

## Sand Crystals

### UNDEFORMED SAND CRYSTALS

A sand crystal (pl. 2*A*) consists of a large single crystal of calcite that poikilitically encloses detrital grains. The undeformed sand crystals used in this study are characterized as follows:

| | Per Cent (by Volume) |
|---|---|
| 1. Mineral composition: | |
| Calcite | 38 |
| Quartz | 25 |
| Feldspar | 22 |
| Rock fragments | 15 |
| Garnet | Trace |

2. The average number of contacts per detrital grain as measured in thin section is 0.71.

3. The calcite crystal is undeformed; that is, no twin lamellae are developed.

4. The detrital grains are relatively unfractured: The fracture index is 111 (see table 1, n. †).

5. There is no marked dimensional or crystallographic orientation of the detrital grains.

### DEFORMATION FAVORABLE FOR TWIN GLIDING

#### EXPERIMENTAL DEFORMATION

Cylinders $\frac{1}{2}$ inch in diameter and 1 inch long were cored from the sand crystals parallel and perpendicular to $c_v$ of the calcite and were deformed dry under the conditions listed in table 1, columns (1)–(4). The ultimate strengths (table 1, col. [5]) were taken from the stress-strain curves of figure 4. Descriptions of the experimental technique and apparatus are given by Handin (1953) and by Handin and Hager (1957, 1958). The cylinders were loaded to promote twin gliding in the calcite crystal, that is, compressed perpendicular to or extended parallel to $c_v$, respectively.

#### PETROGRAPHIC OBSERVATIONS OF DEFORMED SPECIMENS

All deformed specimens are characterized by at least two sets of twin lamellae parallel to $e\{01\bar{1}2\}$ in calcite and by relatively planar microfractures in detrital grains. Both the spacing index of twin lamellae and the index of fracturing in grains tend to increase with increased strain (table 1, cols. [7] and [8]). In all specimens the great majority of microfractures tend to lie perpendicular to the direction of $\sigma_3$ and thus, by definition, are extension fractures (in compression tests $\sigma_2 = \sigma_3$) and fractures are distributed radially and parallel to $\sigma_1$. The spacing and orientation of the microfractures are independent of mineralogy and, in quartz grains, are independent of crystallography. In addition, specimens 878, 877, and 915 exhibit microscopic and/or macroscopic shear zones marked by granulation of the detritus and calcite. These zones are inclined from 26° to 38° to $\sigma_1$.

*Specimen 878*.—Twin lamellae are developed parallel to two of the three potential *e* twin planes. The average spacing index (99) is low compared to those of the other specimens. A macroscopic shear zone is inclined at 33° to $\sigma_1$. Microfractures are inconspicuous, and those that do occur are confined to the shear zone. This is reflected by a low fracture index (126). Although the

## TABLE 1

### Experimental Conditions and Data

| Specimen | Compressed or Extended (1) | Confining Pressure (Bars) (2) | Temper-ature (° C.) (3) | Total Strain (Per Cent) (4) | Ultimate Strength* (Bars) (5) | Remarks (6) | Fracture Index† (7) | Twin-Lamellae Spacing Index‡ (8) |
|---|---|---|---|---|---|---|---|---|
| | | | | **Sand Crystals Deformed Favorably for Twin Gliding** | | | | |
| Undeformed | | | | | | | 111 | 0 |
| 878 | Comp. | 1,000 | 150 | 1.7 | 515 | Sheared 33° to $\sigma_1$ | 126 | 99 |
| 915 | Ext. | 5,000 | 300 | 5.1 | 3,600 | Experiment ended before fracture | 219 | 212 |
| 877 | Comp. | 2,000 | 300 | 8.5 | 4,350 | Sheared 30° to $\sigma_1$ | 212§ | 297 |
| 911 | Ext. | 2,000 | 300 | 13.5 | 1,560 | Sheared 30° to $\sigma_1$ | 288 | 315 |
| | | | | **Sand Crystals Deformed Unfavorably for Twin Gliding** | | | | |
| 1046 | Comp. | 1,000 | 150 | 2.9 | 2,290 | Sheared 28° to $\sigma_1$ | 136 | 22 |
| 1049 | Comp. | 2,000 | 300 | 22.1 | 6,040 | Incipient shear 35° to $\sigma_1$ | 300 | 153 |
| | | | | **Calcite-Cemented Sandstones** | | | | |
| Undeformed | | | | | | Tensleep | 114 | 0 |
| Undeformed | | | | | | Supai | 114 | 0 |
| 724 | | 1,000 | 150 | | | Confining pressure only | 115 | 0 |
| 763 | Ext. | 1,000 | 150 | 2.6 | 1,160 | Broke near center | 114 | 0 |
| 745 | Ext. | 2,000 | 150 | 2.9 | 1,690 | Experiment ended before fracture | 117 | 22 |
| 762 | Comp. | 1,000 | 150 | 3.9 | 4,660 | Sheared 29° to $\sigma_1$ | 169 | 212 |
| 725 | Comp. | 1,000 | 150 | 5.9 | 4,800 | Sheared 30°–35° to $\sigma_1$ | 184 | 152 |
| 778 | Comp. | 2,000 | 300 | 9.2 | 2,040 | Sheared 29° to $\sigma_1$ | 189 | 238 |
| 780 | Comp. | 5,000 | 300 | 10.1 | 6,890 | Experiment ended before fracture | 203 | 302 |

* Ultimate strength, as defined by Handin and Hager (1957), is the maximum ordinate of the stress-strain curve.

† Based on fracturing in four hundred grains per specimen as follows: Per cent unfractured grains ×1, plus per cent of grains with 1–5 fractures ×2, plus per cent with 6–10 fractures ×3, plus per cent with greater than 10 fractures ×4, plus per cent of demolished grains (grain shape obliterated) ×5, ×100 (Borg, Friedman, Handin, and Higgs, 1960, p. 159). Index may vary from 100 to 500. The method is subjective, but indexes determined by one operator can be used to compare relative amounts of fracturing from specimen to specimen.

‡ Based on the number of lamellae per mm. when viewed on edge and measured along a line normal to the twin planes.

§ A macroscopic shear zone, probably containing highly fractured and demolished grains, was destroyed during sectioning. It is reasonable to assume that the index for this specimen would have been higher if grains along this zone could have been counted.

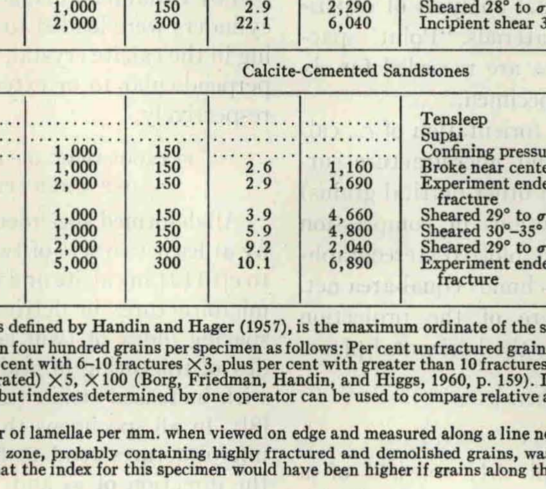


Fig. 4.—Stress-strain curves for sand crystals deformed favorably for twin gliding

microfractures are few in number, they are strongly oriented subnormal to $\sigma_3$ and nearly parallel to $\sigma_1$; that is, they are extension fractures (fig. 5, *a*).

*Specimen 915.*— Three sets of twin lamellae are developed with an average spacing index of 212. Fractured detrital grains are found throughout the specimen, and the fracture index (219) is markedly higher than that of specimen 878. Moreover, the microfractures tend to lie perpendicular to $\sigma_3$ (fig. 5, *b*). No shear zone is developed.

*Specimen 877.*—Three sets of twin lamellae are developed with an average spacing index of 297. Microfractures occur throughout the specimen, and again are oriented as extension fractures (fig. 5, *c*). The fracture index (212) probably represents a minimum value (see table 1, n.§). A macroscopic shear zone inclined at 38° to $\sigma_1$ was observed prior to sectioning. Three instances of intragranular internal rotation were observed in this specimen; that is, the twin lamellae formed early were rotated to irrational positions by twin gliding on another set of lamellae formed later in the deformation. Since the position of $\sigma_1$ is known in the experiment, it is possible to calculate the average strain of each specimen (Turner, Griggs, and Heard, 1954, p. 900). The strains in the three different fields of view are 6.8, 7.6, and 10.6 per cent, respectively—average, 8.3 per cent. The total strain, measured experimentally, is 8.5 per cent.

*Specimen 911.*—The same fabric elements that characterize the other specimens are more strongly developed in specimen 911 (pl. 1). From bottom to top, the specimen can be divided into slightly deformed, moderately deformed, and highly deformed areas. The calcite crystal within the slightly deformed and moderately deformed areas exhibits three sets of twin lamellae. The spacing index of each of these sets varies from one field of view to another, but usually the three sets are equally well developed; the average index is 315. The index increases toward the highly deformed, necked portion of the specimen. In any field of view, the index of a given twin set tends to be greater near the detrital-grain boundaries than in the central portion of an interstitial area (pl. 2*B*, *d*). In the highly deformed area calcite is characterized as follows:

1. Three twin sets are recognizable, although spacing of lamellae is predominantly dense, that is, >400 per mm. Undulatory extinction and bent lamellae are common.
2. Narrow areas of very fine-grained calcite gouge have developed along shear zones.
3. A very fine- to fine-grained mosaic of granulated calcite—a deformation mosaic—has developed throughout the area.

The detrital grains are fractured (index 288), except for those in the triangular area at the base of the cylinder in the "shadow" of the end cup (pl. 1). Except for demolished grains, most quartz, feldspar, and garnet grains and rock fragments exhibit one set of many subparallel microfractures. The microfracture surfaces are strikingly planar (pl. 2*B*, *a*, *b*, and *c*). The number of microfractures per set increases from slightly deformed to moderately deformed to highly deformed areas; in the highly deformed portion, "demolished" grains are commonly smeared out along shear zones. Most microfractures completely cross the host grain, but they may die out within the grain. A 5°–15° rotation of fragments between microfracture surfaces can sometimes be seen if the host grain is at extinction. This phenomenon and the play of light on the microfracture surfaces cause some grains to exhibit "pseudolamellae" of slightly different optical orientation.

The angular relationship between the normals to microfracture surfaces and the $c_v$ of the host quartz grains is illustrated in figure 6. There is a slight tendency for the surfaces to parallel ***r*** or ***z***. That this relationship is non-random may be demonstrated by comparing the histogram with one representing random distribution as shown in figure 6, *a*.

The microfractures show a strong tendency to lie perpendicular to the known position of $\sigma_3$ (fig. 7). The few microscopic shear zones occur at approximately 30° to $\sigma_1$ (pl. 1 and 2*B*, *c*).

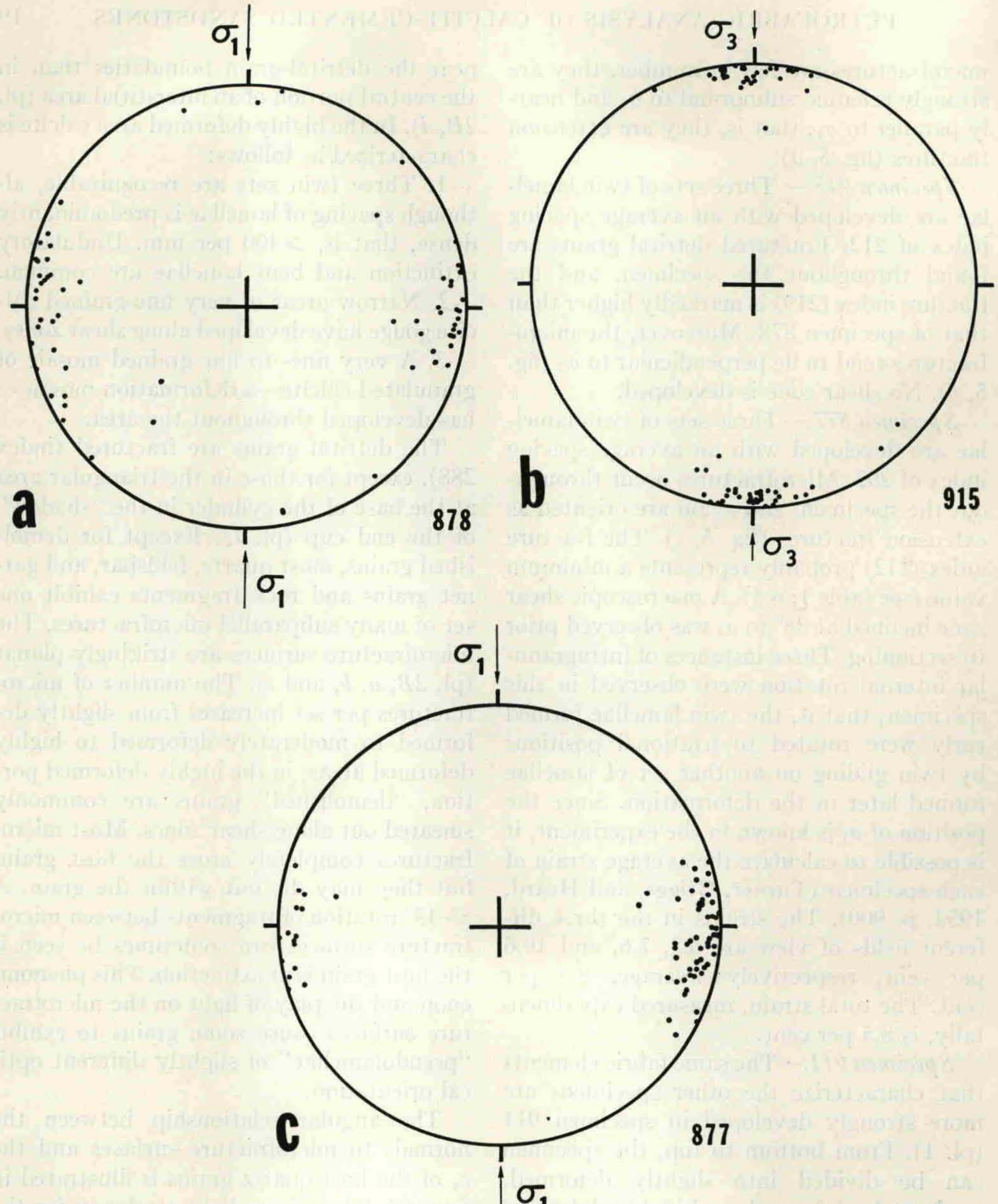


FIG. 5.—Diagrams illustrating orientation of microfractures with respect to load axis for specimens 878, 915, and 877. Plane of each diagram is parallel to long axis of deformed cylinder. *a*, specimen 878, normals to 63 sets of microfractures in fifty detrital grains. *b*, specimen 915, normals to 64 sets of microfractures in fifty detrital grains. *c*, specimen 877, normals to 69 sets of microfractures in fifty detrital grains.

---

PLATE 1

Photograph shows thin section cut parallel to the axis of deformed, necked cylinder. $\sigma_3$ is vertical, and $\sigma_1$ is horizontal. Area of thin section is approximately one-half of total specimen; i.e., cylinder broke just above the necked region when removed from its copper jacket. Planar fractures in detrital grains are oriented predominantly perpendicular to $\sigma_3$, and twin lamellae in the calcite crystal are visible. Slightly deformed, moderately deformed, and highly deformed sectors of the clyinder are indicated. Crossed nicols, $\times 10$.

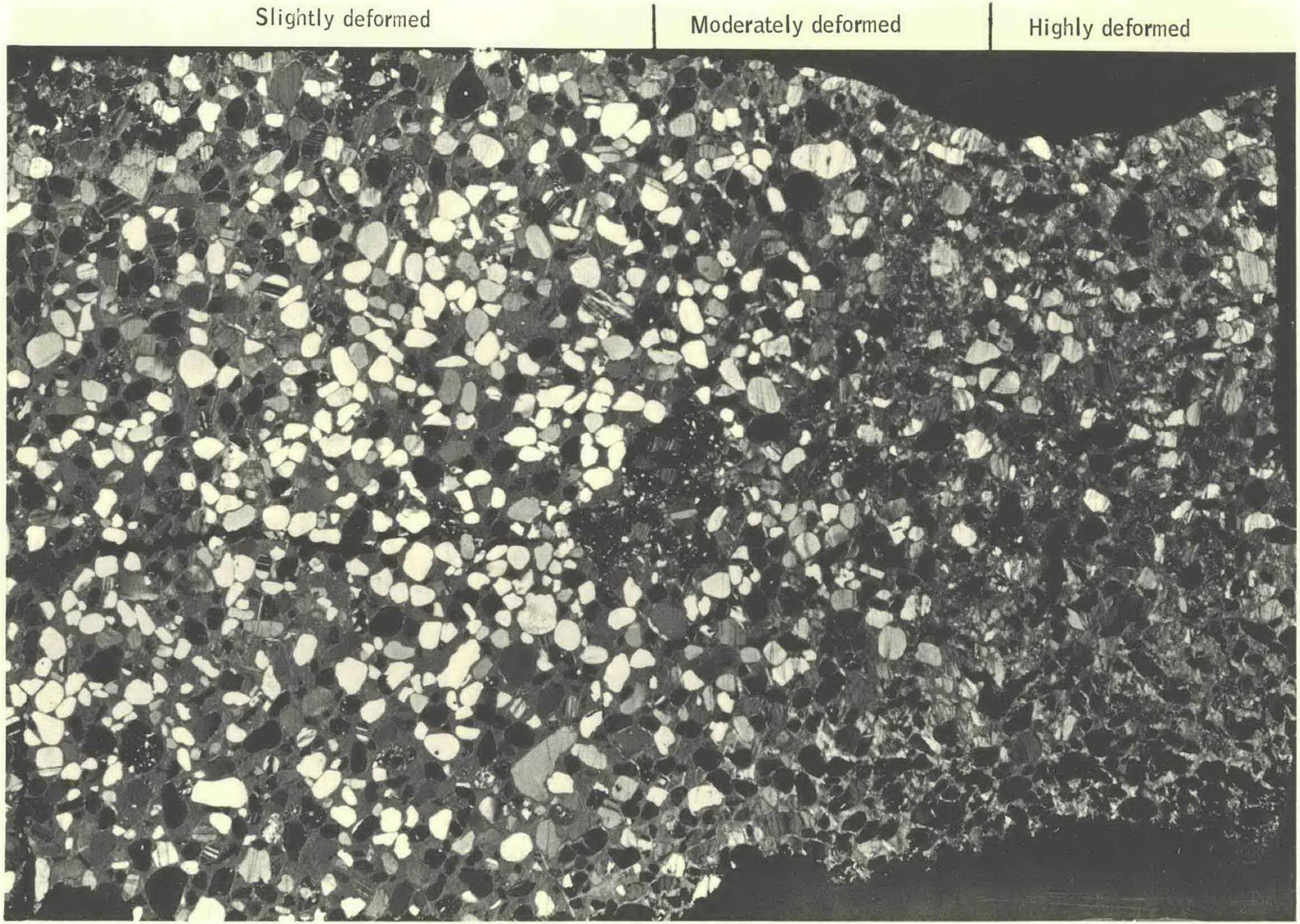


Photograph of Specimen 911, thin section


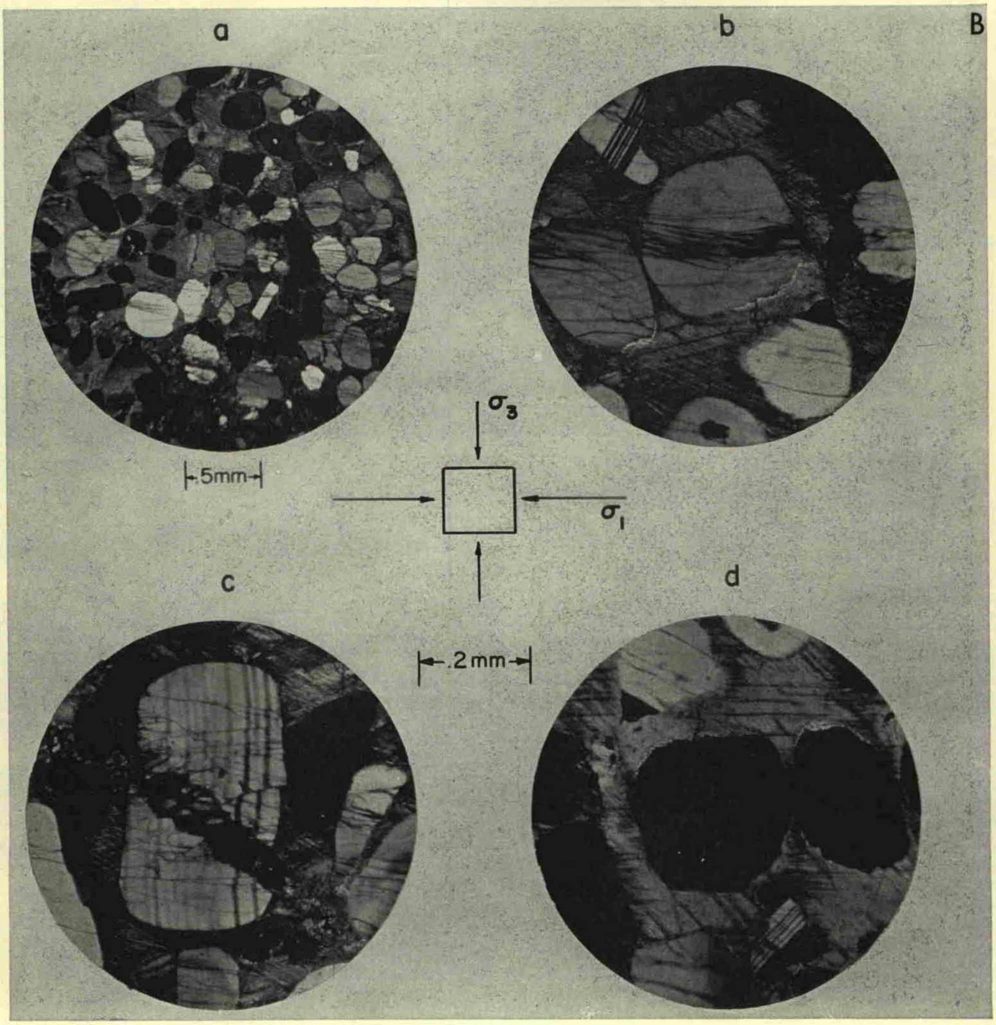


Sand crystals and photomicrographs of details of specimen 911

### DEFORMATION UNFAVORABLE FOR TWIN GLIDING

#### EXPERIMENTAL DEFORMATION

Cylinders 1046 and 1049 were oriented unfavorably for twin gliding during deformation. Accordingly, it is instructive to compare the stress-strain curves and the deformation features produced in these tests with those for specimens 878 and 877, which were oriented favorably for twinning. Experimental conditions for deformation of the four specimens are listed in table 1, columns (1)–(5).

#### STRESS-STRAIN RELATIONSHIPS

Stress-strain curves for the four experiments are shown in figure 8. Although the total strain for each specimen is different, it is possible to compare the strengths of the specimens at a given percentage of strain for each set of experimental conditions. Thus, specimens 1046 and 1049 can be compared with specimens 878 and 877, respectively. At 1.7 per cent strain, specimen 1046 is 3 times as strong as specimen 878; and at 8.5 per cent strain, specimen 1049 is 1.4 times stronger than specimen 877. Both relationships are consistent with the greater strength of a calcite crystal loaded parallel to $c_v$, that is, in a direction unfavorable for twin gliding.

#### PETROGRAPHIC OBSERVATIONS AND COMPARISONS

Specimen 1046 exhibits a macroscopic shear zone or fault that is inclined at 28° to the greatest principal stress ($\sigma_1$). A fine-grained gouge of highly fractured and demolished detrital grains and pulverized calcite marks the shear zone. Detrital grains are generally slightly fractured. Grains adjacent to the shear zone are more highly fractured. The over-all fracture index is 136 (table 1, col. [7]). Nearly all the microfractures are oriented parallel to $\sigma_1$ and accordingly are extension fractures (fig. 9, *a*).

The calcite crystal in specimen 1046 contains a few *e* twin lamellae, traces of $r\{10\bar{1}1\}$ cleavage planes, and extension fractures. The twin lamellae (spacing index is 22; see table 1, col. [8]) are developed only adjacent to the macroscopic shear zone and to fractured detrital grains. Where the grains are unfractured, the calcite is untwinned. Cleavage planes ($r\{10\bar{1}1\}$) are common throughout the specimen, although they are best developed adjacent to the shear zone.[12] In addition, the calcite crystal contains fractures oriented parallel to $\sigma_1$, (fig. 9, *a*, and pl. 3*A*). The fractures are common throughout the specimen but, like the twin lamellae and *r* plates, are best developed adjacent to the shear zone. Although extension fractures in calcite are not common, they probably developed here because the crystal was loaded unfavorably for twin gliding.

It is interesting to compare the fracture indexes and twin-lamellae spacing indexes for specimens 1046 and 878 (table 1, cols. [7] and [8]). The fracture index for specimen 1046 (136) is slightly higher than that for specimen 878 (126). This probably reflects the higher strain (2.9 per cent) of specimen 1046. On the other hand, the twin-lamellae spacing index for specimen 878 (99), loaded favorably for twin gliding, is 4.5 times as high as that for specimen 1046 (22). This no doubt reflects the difference between the

[12] The possibility of translation gliding parallel to *r* cannot be excluded. Translation on *r* with a negative sense of shear is a known mechanism in calcite, and in a calcite crystal compressed parallel to $c_v$, there is a high resolved shear stress parallel to *r* planes and in the correct sense for translation gliding. However, since translation gliding does not produce visible lamellae, and since there has been no internal rotation, it cannot be substantiated.

---

PLATE 2

*A*, Cluster of sand crystals.

*B*, Orientation of principal stresses during deformation is shown in center of figure. In *a*, *b*, *c*, and *d*, planar microfractures are illustrated that are developed in parallel sets oriented perpendicular to $\sigma_3$ and parallel to $\sigma_1$; i.e., they are extension fractures. In *c*, a microshear zone in a feldspar grain is shown. The shear zone is inclined at 30° to $\sigma_1$. In *b* and *d*, twin lamellae in the calcite crystals are visible. Crossed nicols.

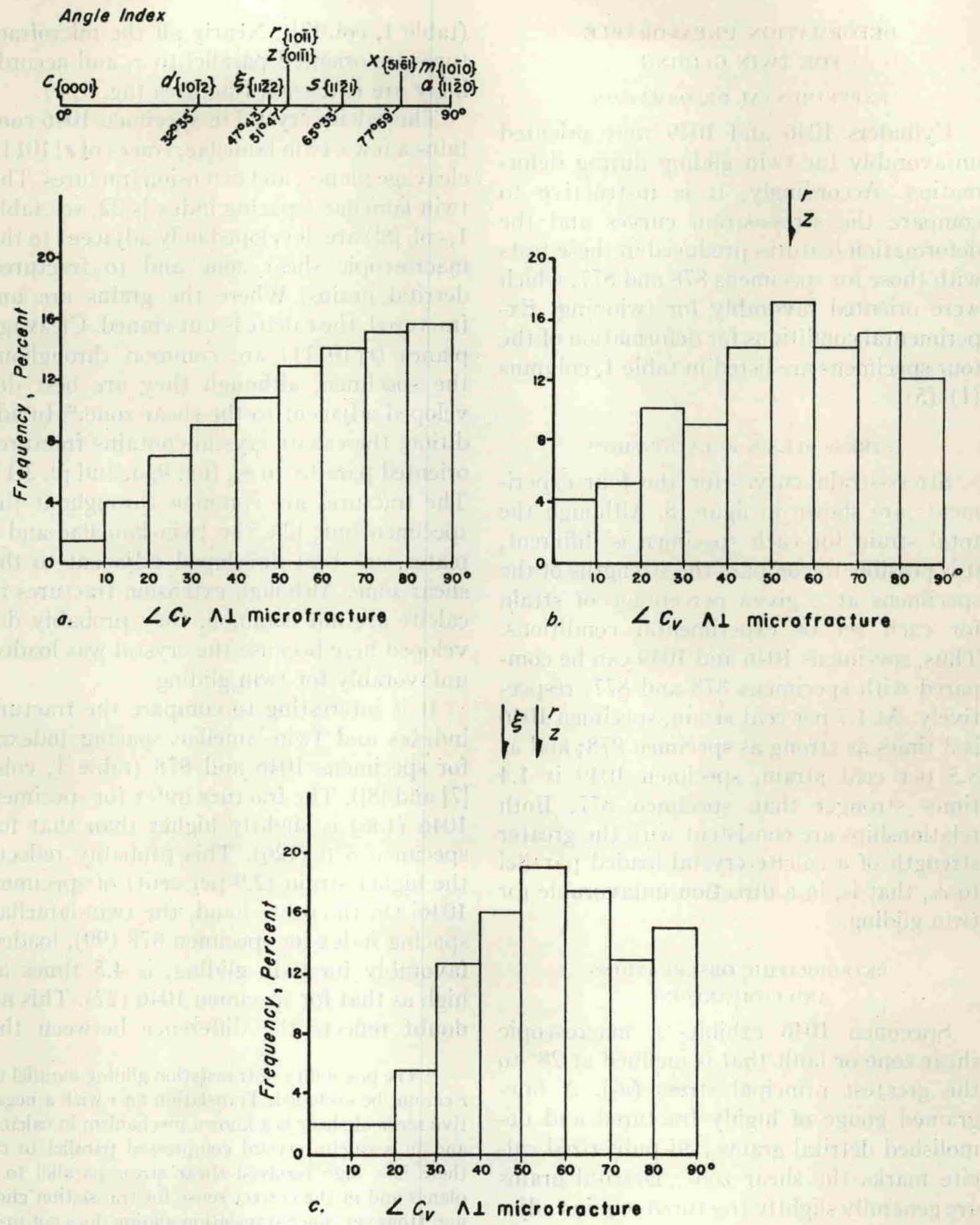


FIG. 6.—Histograms of distribution of angles between normal to microfractures and $c_V$ in host quartz grains. *a*, random distribution (Bloss, 1957):

$$P = 100 \int_{\theta_1}^{\theta_2} \sin\ \theta d\theta = 100(\cos\ \theta_1 - \cos\ \theta_2)$$

$$\theta_2 - \theta_1 = \text{cell width in degrees}\ .$$

Angle index shows angles between $c_V$ and common forms in quartz. (This index applied to all diagrams of fig. 6.) *b*, specimen 911; data are from 111 fracture sets in 100 quartz grains. *c*, specimen 725. Data are from 348 fracture sets in 200 quartz grains.

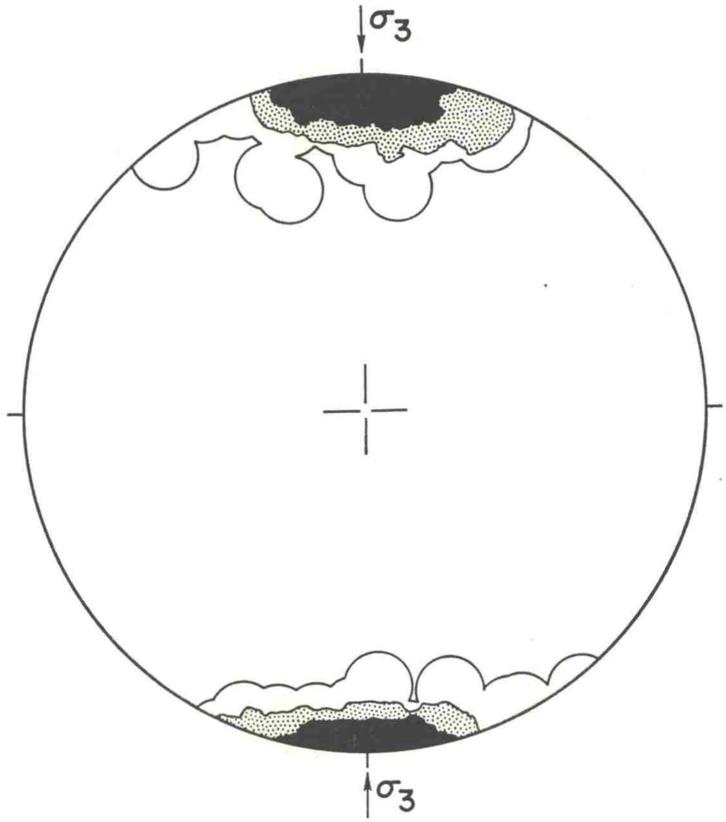


FIG. 7.—Specimen 911. Diagram of normals to 143 fracture sets in 129 detrital grains, of which 100 are quartz. Contours: 0.7, 3.5, and 10 per cent per 1 per cent area; 40 per cent maximum per 1 per cent area.

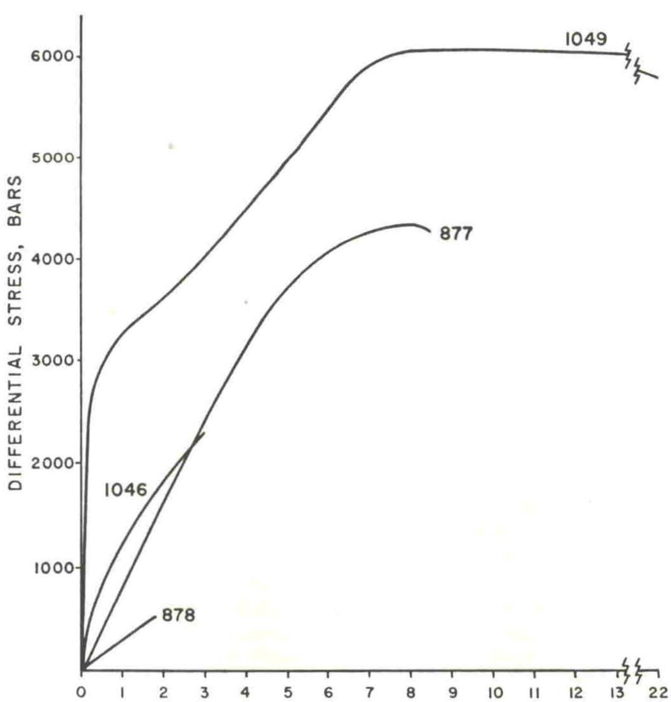


FIG. 8.—Stress-strain curves for specimens 878, 1046, 877, and 1049

orientation of the load axis with respect to the calcite crystal in the two specimens.

Specimen 1049 exhibits an incipient shear zone 0.1 inch wide that is inclined at 35° to $\sigma_1$. The zone is marked by a deformation mosaic in the calcite. Detrital grains are highly fractured within the zone but not more so that outside. Little if any shearing movement has taken place along the zone, as is evident from the lack of offset at the cylinder boundaries. In addition, the specimen exhibits a clockwise external rotation of 10°–15° caused by constraint of the steel end cups. The detrital grains are highly fractured throughout the specimens (fracture index is 300). The microfractures are parallel to $\sigma_1$, (fig. 9, *b*). The microfractures reflect the external rotation of the cylinder and therefore formed prior to the kinking.

The calcite crystal in specimen 1049 exhibits twin lamellae (index is 153), undulatory extinction, a few $r\{10\bar{1}1\}$ planes, and some extension fractures. In areas of the specimen outside the incipient shear zone, the calcite is characterized as follows:

1. Twin lamellae are best developed adjacent to fractured detrital grains and die out into the centers of the interstices.

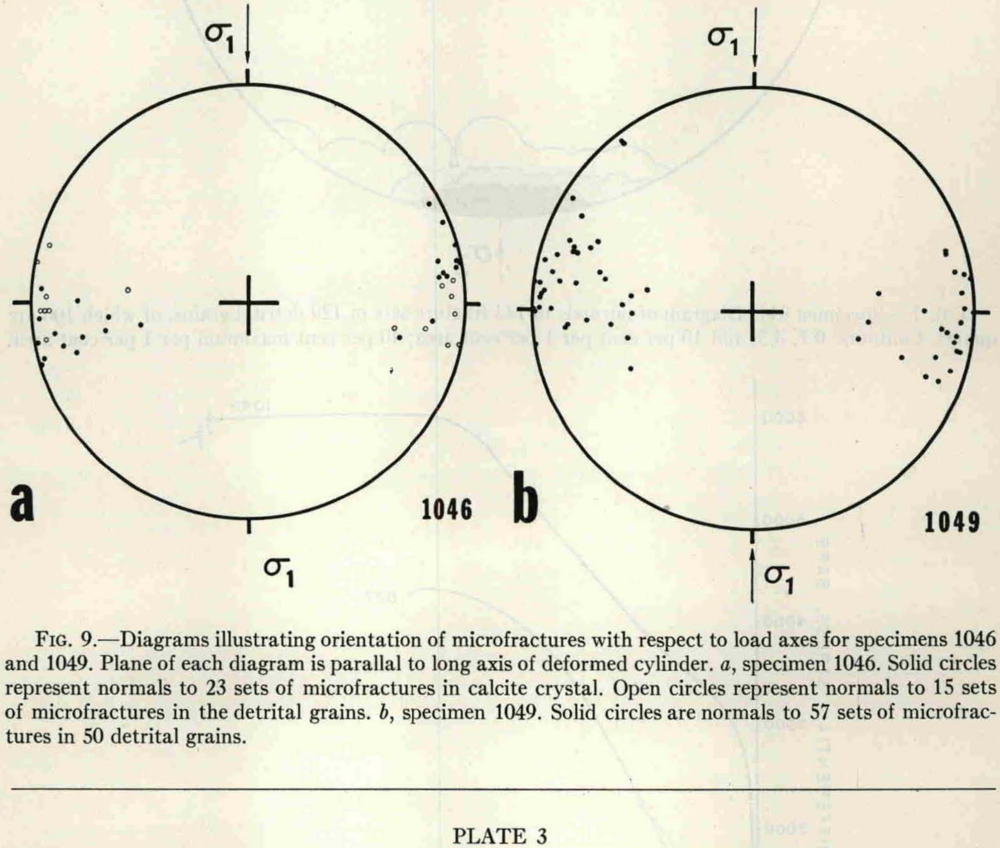


FIG. 9.—Diagrams illustrating orientation of microfractures with respect to load axes for specimens 1046 and 1049. Plane of each diagram is parallal to long axis of deformed cylinder. *a*, specimen 1046. Solid circles represent normals to 23 sets of microfractures in calcite crystal. Open circles represent normals to 15 sets of microfractures in the detrital grains. *b*, specimen 1049. Solid circles are normals to 57 sets of microfractures in 50 detrital grains.

---

PLATE 3

*A*, Photomicrograph of extension fractures in calcite crystal and in detrital grains of specimen 1046. The fractures are oriented with respect to the principal stress axes as shown. Crossed nicols.

*B*, Photomicrographs showing details in specimen 725 (pl. 4). *a*, Photomicrograph shows microfractures in the detrital grains and the through-going shear zone. It is oriented such that $\sigma_1$ is N.-S. and $\sigma_3$ is E.-W. Crossed nicols. *b* and *c*, Photomicrographs illustrate twin lamellae in deformed calcite cement, located at the center of each field of view. Photomicrographs were taken with the thin section mounted on the universal stage so that the twin lamellae at the center of *c* are tilted on edge. One nicol.

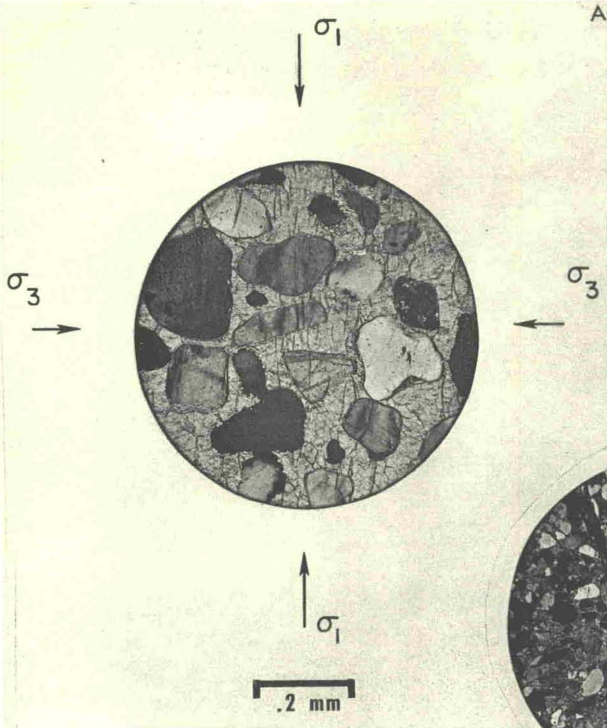


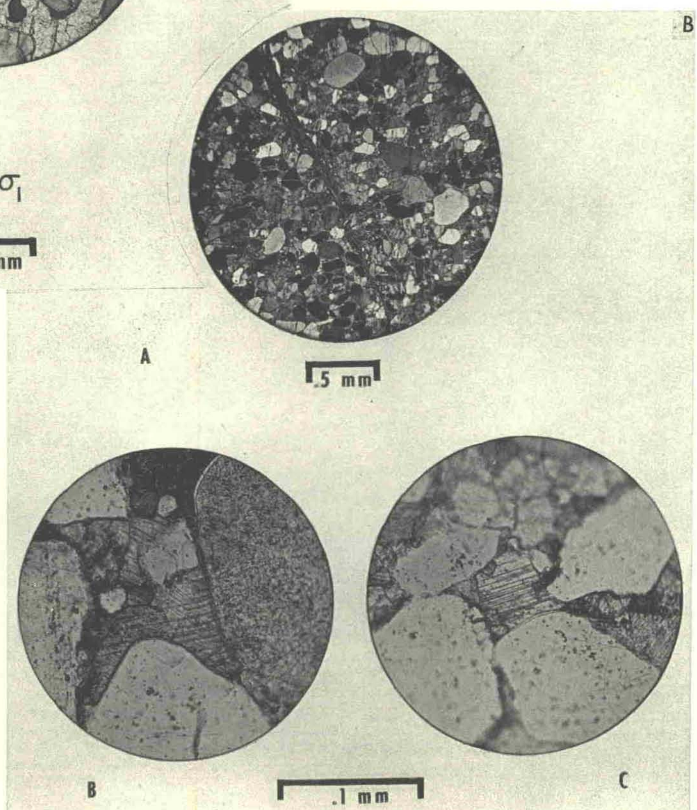


Thin section cut of specimen 725

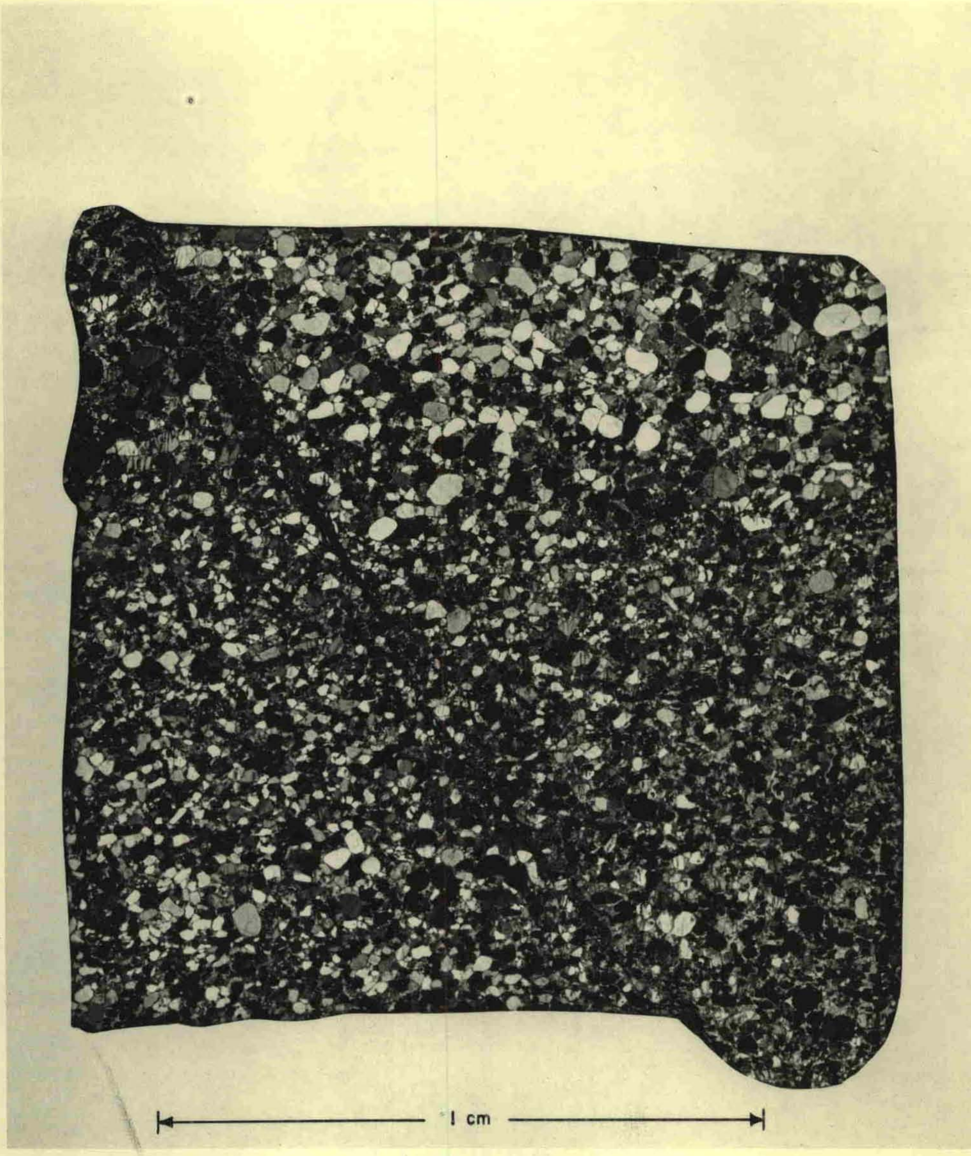


Photomicrographs of specimens 1046 and specimen 725

2. Lamellae are commonly bent about detrital grains. This is accompanied by undulatory extinction in the area of bending so that the rational relationship between lamellae and $c_v$ is maintained. Maximum displacement of $c_v$ occurs immediately adjacent to detrital grains.

3. Lamellae are best developed on those sides of fractured grains that are subparallel to the microfracture surfaces. Commonly, only a few lamellae are developed on those sides of the grains that are normal to the microfracture surfaces (fig. 10).

4. In the untwinned portions of the crystal, some *r* cleavage planes and extension fractures have developed. The extension fractures are parallel to, and sometimes continuous with, those in neighboring detrital grains.

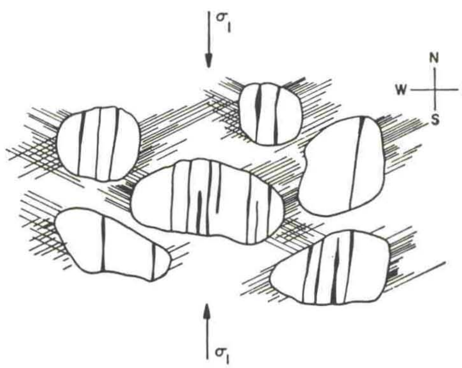


FIG. 10.—Sketch of fractured detrital grains and twin lamellae in calcite crystal. Twin lamellae are best developed on east and west sides of fractured grains and tend to die out into the interstices. Few lamellae are developed north and south of grains.

It is also interesting to compare the fracture indexes and twin-lamellae spacing indexes for specimens 1049 and 877. The fracture index of specimen 1049 (300) is higher than that for specimen 877 (212). This again probably reflects the greater strain of specimen 1049. The twin-lamellae spacing index of specimen 1049 (153) is about half that in specimen 877 (297), even though specimen 1049 has been strained about 2.7 times as much as specimen 877. There is no doubt that this difference is associated with the fact that specimen 1049 was loaded unfavorably for twin gliding.

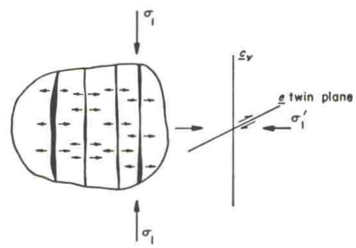


FIG. 11.—Schematic explanation of development of twin lamellae in 1046 and 1049. Detrital grain exhibits extension fractures. Movement on extension fractures is normal to fracture surfaces. This sets up a local stress ($\sigma_1'$) which produces a high resolved share stress parallel to the *e* twin plane and in the correct sense for twin gliding.

*Discussion.*—It is apparent that specimens 1046 and 1049 are stronger and exhibit fewer twin lamellae than specimens 878 and 877. However, if specimens 1046 and 1049 were loaded unfavorably for twin gliding, why should they contain any twin lamellae? In both specimens the twin lamellae are well developed only adjacent to detrital grains with extension fractures. Theoretically, movement associated with extension fractures is normal to the walls of the fracture and creates a local stress situation in which $\sigma_1$ is oriented to produce a high resolved shear stress in the proper sense for twin gliding parallel to the *e* planes in the adjacent calcite crystal (fig. 11). As the critical resolved shear stress is low, the local

PLATE 4

Photograph shows thin section cut parallel to the long axis of the deformed cylinder. The greatest principal stress ($\sigma_1$) is N.–S. The macroscopic shear zone containing gouge of quartz fragments and calcite cement is inclined at about 30° to $\sigma_1$. Fractures in detrital grains are predominantly parallel to $\sigma_1$; i.e., they are extension fractures. Crossed nicols.

stress can induce twin gliding despite the orientation of $\sigma_1$ on the specimen as a whole.

It is also important to emphasize that with increased strain (table 1, cols. [4] and [8]) the number of microfractures tends to increase independently of the orientation of the load axis with respect to the specimen. Also, in specimen 1046, all deformation features are best developed adjacent to the macroscopic shear zone.

cent (capillary-pressure determination); the low porosity minimizes the deformation effects caused by the collapse of voids upon application of confining pressure.

5. Lack of visible evidence of strong compaction: point- and long-grain contacts occur; the average number of contacts per grain is 2.1.

6. Unfractured detrital grains: the fracture index in the quartz grains is 114; $c_v$ of

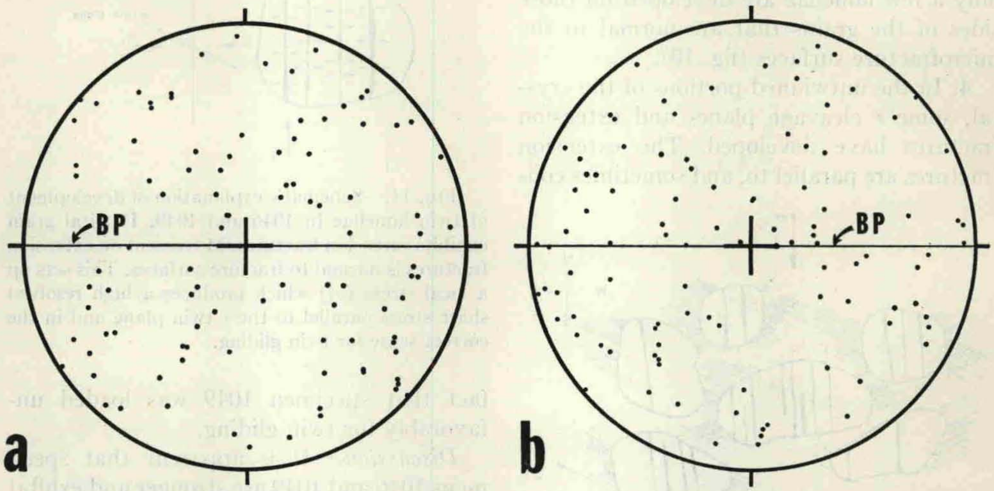


FIG. 12.—Diagrams show random orientation of 100 $c_v$ in calcite cement (*a*) and in quartz grains (*b*) of undeformed Tensleep sandstone. Plane of each diagram is normal to bedding plane (*BP*) as indicated.

quartz grains are randomly oriented (fig. 12, *b*).

## CALCITE-CEMENTED SANDSTONES

### UNDEFORMED TENSLEEP SANDSTONE

Undeformed Tensleep sandstone is well suited for this study because of its simple mineralogy, grain size, undeformed cement, unfractured detrital grains, and low porosity. It is characterized by:

1. Simple composition: the rock contains 69 per cent detrital grains (62 per cent quartz) and 31 per cent calcite cement.

2. Suitable crystal size: half the cement (15.8 per cent of the rock) is ideal for universal-stage study; that is, crystals are between 0.1 and 0.4 mm. in diameter.

3. Undeformed cement: only 2 per cent of the calcite crystals exhibit any twin lamellae; $c_v$ of the calcite are randomly oriented (fig. 12, *a*).

4. Low porosity: the porosity is 3.4 per

### UNDEFORMED SUPAI SANDSTONE

Undeformed Supai, which is similar to the Tensleep except for higher porosity and fewer contacts per grain, is characterized by:

1. Simple composition: the rock is composed of 55 per cent detrital grains (53 per cent quartz), 35 per cent calcite cement, and 10.5 per cent void space.

2. Calcite cement: the cement is almost entirely undeformed; the crystals range from 0.1 to 0.3 mm. in diameter; $c_v$ are randomly oriented.

3. Porosity: the porosity is 17.5 per cent (capillary-pressure determination).

4. Lack of compaction: the average number of contacts per grain is 1.1.

5. Previous deformation features: the fracture index is 114; small, incipient shear zones occur, with small amounts of gouge; $c_v$ of quartz grains are randomly oriented.

### EXPERIMENTAL DEFORMATION

Cylinders $\frac{1}{2}$ inch in diameter and 1 inch long were cored perpendicular to the bedding and with regard to reference markings so that similarly oriented thin sections of undeformed and deformed specimens could be compared. The cylinders are deformed dry under the conditions listed in table 1, columns (1)–(4). Specimens 778 and 780 are from the Supai sandstone; all others are from the Tensleep sandstone. Ultimate strengths (table 1, col. [5]) were taken from the stress-strain curves of figure 13.

### PETROGRAPHIC OBSERVATIONS OF DEFORMED SPECIMENS

All specimens, except 724 and 763, are characterized by twin lamellae parallel to $e\{01\bar{1}2\}$ in the calcite, by microfractures in the detrital grains, and by macroscopic shear zones. Both twin-lamellae spacing and microfracture indexes tend to increase with increased strain (table 1, cols. [7] and [8]). Generally, the microfractures tend to lie perpendicular to $\sigma_3$; that is, they are extension fractures. The orientation and spacing of the microfractures are independent of mineralogy and, in quartz grains, are independent of crystallography. Macroscopic shear zones are inclined between 29° and 35° to $\sigma_1$ (pl. 4).

*Specimen 724.*—This specimen was subjected to a uniform pressure of 1,000 bars, thereby simulating about 15,000 feet of overburden. The cylinder suffered no permanent deformation. Detrital grains are unfractured (index is 115), and the average number of contacts per grain is unchanged (2.1). In addition, the calcite cement is undeformed; the twin-lamellae spacing index is the same as that of the undeformed material (0).

*Specimen 763.*—This specimen was extended 2.6 per cent under 1,000 bars confining pressure, but no evidence of the strain is apparent in the thin section (i.e., no microfractures or twin lamellae formed).

*Specimen 745.*—This specimen was extended 2.9 per cent under 2,000 bars confining pressure, and some evidence of the deformation is apparent. Some detrital grains exhibit microfractures (index is 117), and the calcite cement exhibits a few twin lamellae (spacing index is 22).

*Specimens 762, 725, 778, and 780.*—These specimens were compressed 3.9, 5.9, 9.2, and 10.1 per cent, respectively (table 1, col. [4]). They contain similar, pronounced deformation features that are characterized as follows:

1. Macroscopic shear zones occur in specimens 762, 725, and 778; they are inclined at 29°–35° to $\sigma_1$ (table 1, col. [6]), as shown in plate 4 for specimen 725. Along these zones, detrital grains have been smeared out to form fine-grained gouge (pl. 3*B*, *a*). In addition, elongate grains along shear zones have been bodily rotated to lie subparallel to the zones. Shearing is not as pronounced in specimen 778 as in specimens 725 and 762. This may be due to a combination of the effects of increased confining pressure and temperature in specimen 778.

2. Highly fractured detrital grains occur throughout all four specimens, as illustrated in plates 3*B* and 4. The fracture index increases with increased strain (table 1, col. [7]). Sets of microfractures are statistically oriented parallel to $\sigma_1$ and normal to $\sigma_3$ (pls. 3*B* and 4 and fig. 14, *a–e*). In thin sections cut perpendicular to the $\sigma_1$ axis, the normals to the microfractures form nearly complete peripheral girdles which are inclined at about 90° to $\sigma_1$ (fig. 14, *a*). The microfracture surfaces themselves, therefore, are subparallel to $\sigma_1$. In these experiments, $\sigma_1 > \sigma_2 = \sigma_3$, and the least principal stress ($\sigma_2 = \sigma_3$) is oriented everywhere about the circumference of the deformed cylinder. Therefore, the normals forming the girdle are also everywhere normal to the least principal stress. In thin sections cut parallel to the $\sigma_1$ axis, the orientation of the microfractures is clearly illustrated (fig. 14, *b–e*). It should be remembered that there is a central blind

spot in these diagrams. The concentrations of normals at nearly right angles to the direction of $\sigma_1$ show that, for the most part, the microfracture surfaces are oriented parallel to $\sigma_1$ and normal to $\sigma_3$. That all the microfractures are not extension fractures is clear from the number of normals that are not inclined at 90° to $\sigma_1$. Those normals inclined between 70° and 50° to $\sigma_1$ probably represent shear fractures. The distribution of microfractures in specimen 780 tends to be more diffuse than in specimens 762, 725, and 778, although extension fractures predominate. This is probably due to the bodily

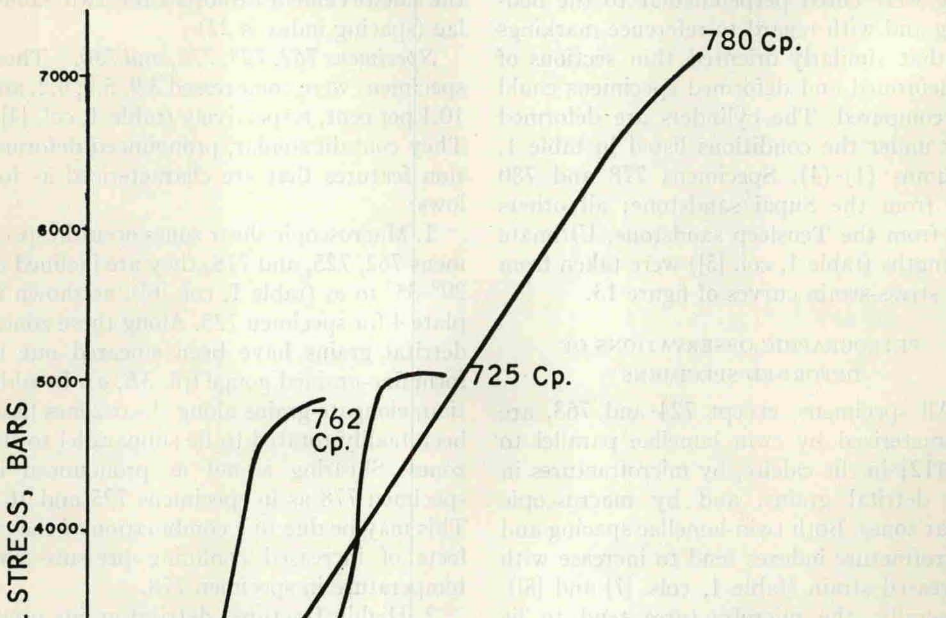


FIG. 13.—Stress-strain curves for calcite-cemented sandstones

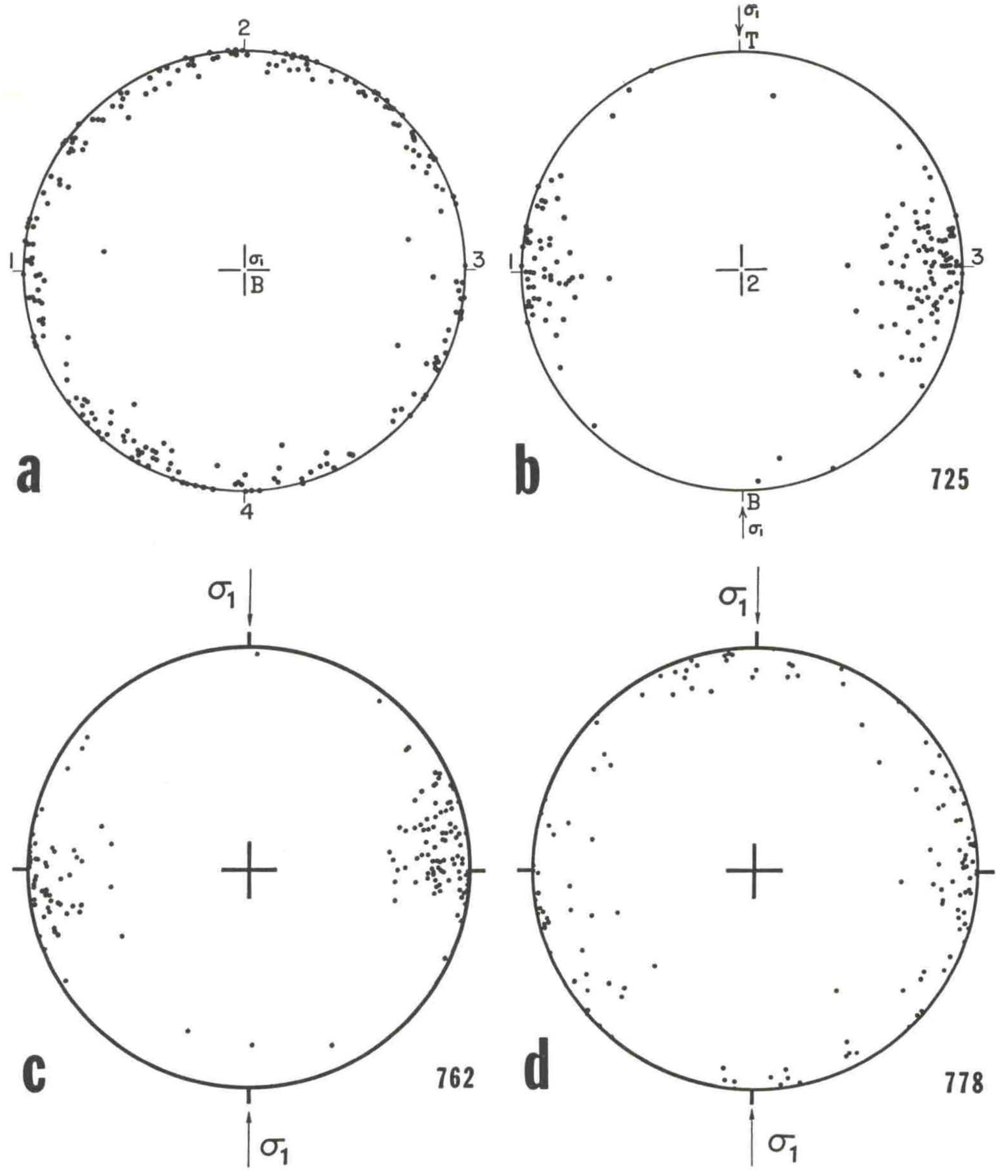


FIG. 14.—*a*, specimen 725. Normals to 198 sets of microfractures in 100 detrital grains. Diagram oriented perpendicular to long axis of deformed cylinder with $\sigma_1$ at the center, at *B*. *b*, specimen 725. Normals to 153 sets of microfractures in 100 detrital grains. Diagram oriented parallel to long axis of deformed cylinder with $\sigma_1$ oriented N.-S. *c*, specimen 762. Normals to 138 sets of microfractures in 100 detrital grains. Diagram is oriented same as in *b*. *d*, specimen 778. Normals to 125 sets of microfractures in 100 detrital grains. Diagram is oriented same as in *b*.

[*Fig. 14 continued on p. 30.*

rotation of the fracture planes away from their initial positions.

There appears to be a slight tendency for the microfractures to form parallel to ***r*** and *z*, as shown in figure 6, *c*, which illustrates the relations between the normals to the microfractures and the $c_v$ in the host quartz grains for specimen 725. This possible crystallographic control of fractures is, however, greatly overshadowed by the marked relationships between the microfractures and the calcite grains exhibit undulatory extinction. This indicates that the grains have been externally rotated during deformation. In the four specimens, twin lamellae are preferentially oriented in contrast to random $c_v$ orientations; normals to the lamellae are clustered within $\pm 45°$ of $\sigma_1$, as illustrated in figure 15, *A* and *B*, for specimens 725 and 780. This indicates that twin gliding takes place only on those sets of twin planes that are favorably oriented with respect to $\sigma_1$.

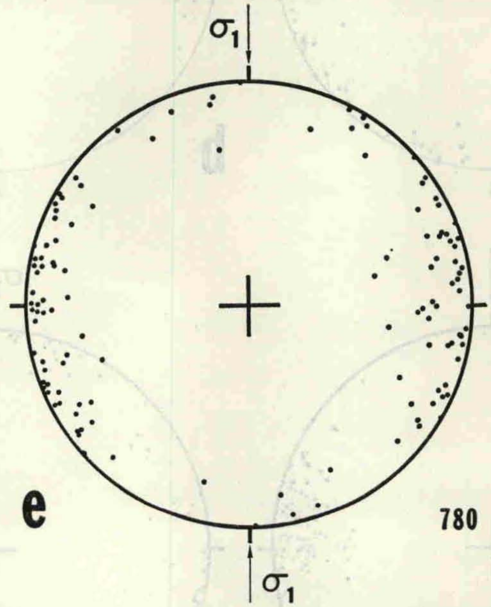


FIG. 14.—*Continued.*—*e*, specimen 780. Normals to 119 sets of microfractures in 100 detrital grains. Diagram is oriented as in *b*. In all diagrams the majority of the microfractures are oriented parallel to $\sigma_1$ and normal to $\sigma_3$; i.e., they are extension fractures.

the principal stresses across the boundaries of each specimen.

3. Twin lamellae are profusely developed in the calcite cement (pl. 3*B*, *b* and *c*). Approximately 85 per cent of the grains exhibit at least one set of twin lamellae, and the average spacing indexes are generally high—212, 152, 238, and 302 for specimens 762, 725, 778, and 780, respectively. Moreover, it is significant that the spacing index generally increases with increased strain, although one reversal was noted in comparing specimens 762 and 725. The twin lamellae in specimen 780 are commonly bent, and

## Discussion of Results

### Relationship of Principal Stress Orientations and Observed Twin Lamellae

The preferential arrangement of twin lamellae relative to $\sigma_1$ in specimens 762, 725, 778, and 780 is significant. Handin and Griggs (1951) assumed that each calcite grain in a monomineralic aggregate would reflect the loads applied to the specimen as a whole rather than the effects of stress concentrations at grain contacts. This was confirmed for marble by Turner and Ch'ih (1951), who showed statistically that for

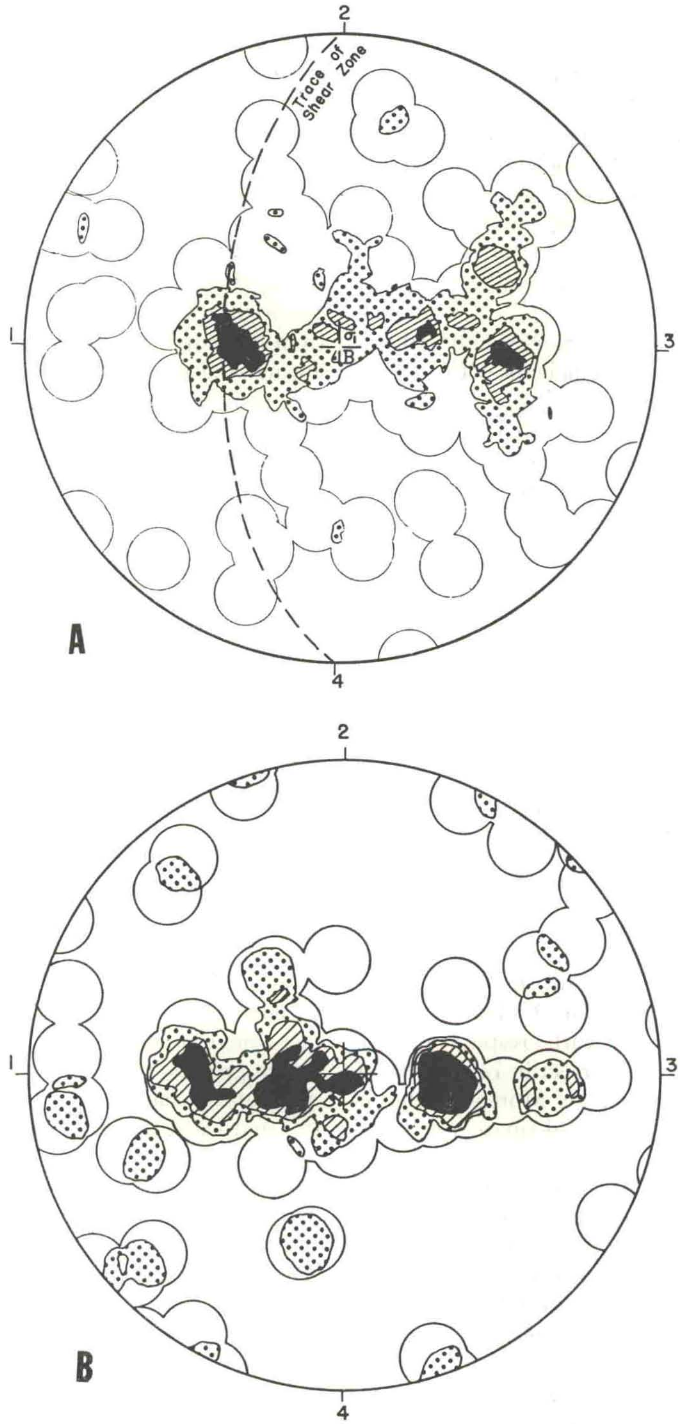


FIG. 15.—*A*, specimen 725. Composite diagram of normals to 102 *e* twin lamellae. The plane of the diagram is perpendicular to long axis of deformed cylinder, and $\sigma_1$ is at the center. Contours: 1, 3, 5, and 7 per cent per 1 per cent area. *B*, specimen 780. Composite diagram of normals to 61 *e* twin lamellae. The plane of the diagram is perpendicular to long axis of deformed cylinder, and $\sigma_1$ is at the center. Contours: 1.66, 3.33, 5.0, and 6.66 per cent per 1 per cent area.

each calcite grain the highest spacing index is correlated with the highest resolved shear-stress coefficient ($S_0$). That is, of the family of three *e* planes, twinning is best developed on that plane for which $S_0$ is highest. If this holds for calcite-cemented sandstones, then on the average the cement also responds to over-all loading instead of to local stresses at grain boundaries.

In specimens 762, 725, 778, and 780, resolved shear-stress coefficients with respect to the known position of $\sigma_1$ were determined for $e_1$, $e_2$, and $e_3$ in each calcite crystal which contained at least one set of twin lamellae. The method is described by Handin and Griggs (1951, p. 866–869, fig. 3). The results are listed in table 2. The direction sense for twinning with respect to the external load axis is correct in 74 per cent of the measured $e_1$ lamellae. Moreover, the $S_0$ values (0.23–0.30) are adequate for twinning. Since the direction sense of twinning and $S_0$ correlate significantly with $\sigma_1$ in each specimen, it is reasonable to conclude that statistically the individual crystals of calcite cement are twinned with respect to the load on each cylinder as a whole rather than to local stress concentrations.

TABLE 2

RESOLVED SHEAR-STRESS COEFFICIENT ($S_0$) DATA

| Conditions | Specimen | | | |
|---|---|---|---|---|
| | 762 | 725 | 778 | 780 |
| *a*) Number of grains measured | 50 | 100 | 50 | 60 |
| *b*) Number of grains exhibiting twin lamellae | 49 | 98 | 50 | 49 |
| *c*) Percentage of grains in which $e_1$ lamellae twinned in correct sense with respect to $\sigma_1$ | 76 | 74 | 76 | 71 |
| *d*) Average $S_0$ on $e_1$ for grains in (*c*) | 0.30 | 0.25 | 0.28 | 0.23 |
| *e*) Percentage of grains (*c*) in which $e_1$ lamellae have the highest $S_0$ for correct sense of gliding when compared to $e_2$ and $e_3$ | 92 | 88 | 89 | 57 |

In specimens 762, 725, and 778, the highest values of $S_0$ are for planes other than those designated as $e_1$ in about 10 per cent of the cases (table 2, row *e*). In specimen 780, true $e_1$ lamellae were not identified in 43 per cent of the cases. Either this plane of highest spacing index is inclined to the thin section at too small an angle to be measurable, or the spacing indexes of two or more of the planes are too high or too nearly equal to permit distinction.

The fact that the calcite cement responds to over-all loading leads to the conclusion that it should be possible to determine average orientations of principal stresses in rocks from measurements of twin lamellae. Following the methods outlined previously, one can plot the compression axes that would be most effective in producing the observed $e_1$ lamellae in specimens 762, 725, 778, and 780 (fig. 16, *a–d*, respectively). For specimens 762, 725, and 778, the "center of gravity" of the highest concentrations in each diagram marks the deduced position of the greatest principal stress ($\sigma_1'$), which is about 20° southeast, 10° north, and 10°–15° southeast, respectively, of the known position of $\sigma_1$ in each specimen. Doubling the strain in specimen 778 sharpens the concentration of compression axes about $\sigma_1$. The distribution of compression axes is more diffuse for specimen 780 than for the other specimens because of the high percentage of incorrectly identified $e_1$ lamellae and because of the external rotations of many of the grains. Even so, there is an obvious grouping of compression axes about the correct position.

The lack of deformation effects in specimen 724, which was subjected only to uniform confining pressure simulating 15,000 feet of overburden, is highly significant. It indicates that uniform pressure alone cannot produce twinned calcite cement or fractured detrital grains in these rocks. Accordingly, the microfeatures suggest the influence of differential loading, that is, tectonism.

### RELATIONSHIP OF PRINCIPAL STRESS ORIENTATIONS AND OBSERVED MICROFRACTURES

Stresses must be transmitted to the individual grains of a sand aggregate through grain contacts. Borg and Maxwell (1956) found that microfractures tended to radiate from point contacts in deformed unconsolidated sand, but in the cemented materials the microfractures are principally of the extension type and tend to transect grains. They are clearly related to the known principal stress axes across the whole rock rather than to local stress concentrations at grain contacts. These results hold at least over the 0–18 per cent porosity range.

### STRESS-STRAIN RELATIONSHIPS

At what differential stress will these deformation features began to develop? As mentioned in the section on previous work, experiments on calcite single crystals have established that the critical resolved shear stress to induce twinning on *e* is low. On the other hand, the breaking strength of quartz in short-time tests at atmospheric pressure and room temperature is extremely high. One might suppose, therefore, that in deformed calcite-cemented sandstones, calcite would twin in response to a very small differential stress, and that quartz would fracture only under a large load. The present work amply demonstrates that this need not be so.

In this regard, it is instructive to compare the stress-strain curves for sand crystals (fig. 4) and calcite-cemented sandstones (fig. 13). In the former, the detrital grains tend to "float" (the average number of contacts per grain in thin section is 0.71) in the calcite crystal, and the porosity approaches zero. In the latter, the higher number of contacts per grain and the higher porosity suggest that calcite tends to occupy interstitial areas surrounded by voids and detrital grains in contact. These differences are reflected by the different shapes of the stress-strain curves from the origin to the onset of yielding. The calcite-cemented sandstones exhibit **S**-shaped curves (fig. 13), which, according to Handin (personal communication), are characteristic of porous rocks deformed under moderate confining pressures. The application of differential pressure collapses pore spaces, so that the initial strain is relatively large. Thereafter, the rock is strained essentially elastically to the yield stress. No visible permanent deformation need be associated with these events. Specimen 763 exhibits a typical **S**-shaped curve, has obtained a maximum differential stress of 1,160 bars at 1,000 bars confining pressure, and yet contains no twin lamellae in the cement or fractures in the detrital grains. These microfeatures are present, however, in specimen 745, which also exhibits an **S**-shaped curve but has obtained a maximum differential stress of 1,690 bars at 2,000 bars confining pressure. Accordingly, microfeatures develop in these extension experiments at differential stresses of between 1,200 and 1,700 bars, if the difference between the confining pressures of the two experiments can be neglected. In the compression experiments permanent deformations are not important until the yield stresses are attained. Accordingly, in specimens 762 and 725 (deformed at 1,000 bars confining pressure and 150° C.), microfeatures begin to form at differential stresses of 4,500 and 4,800 bars, respectively. At higher temperatures, the yield stresses are lower—1,500 and 2,000 bars for specimens 778 and 780, respectively. Clearly, the nature of the tectonic environment would greatly affect the magnitude of the differential stress at which permanent deformation in the rock would begin.

The stress-strain curves for the sand-crystal experiments (fig. 4) show linear relationships between stress and strain up to the yield stresses. Since the porosity of the sand crystal is essentially zero, an **S**-shaped curve would not be expected. Generally, for the same experimental conditions, permanent deformations were recorded at lower differential stresses in the sand-crystal specimens than in the calcite-cemented sandstones. For example, specimen 878 (sand crystal), which was deformed under the same conditions as specimens 762 and 725 (sandstones), exhibits microfeatures in the calcite and in the detrital grains and yet has obtained a maximum differential stress of only 515 bars.

It is reasonable to conclude that the calcite cement in the sandstones tends to be "protected" by surrounding detrital grains in contact. Twinning occurs in the calcite only after the detrital grains begin to fracture. The grains fracture under relatively small loads on the aggregate as a whole, because the stress concentrations at points of contact are very large. However, perhaps surprisingly, the fractures do not radiate from points of contact, but form as if each grain reacted to the forces applied to the aggregate in bulk. From this reasoning, it also follows that for the same confining pressure, twinning and grain-fracturing should take place in the sand crystals at lower differential stresses. Since the grains tend to "float" in the crystal, the calcite is "unprotected" and twins in response to smaller loads. In addition, the detrital grains exhibit fewer contacts per grain, so that the stress concentrations per contact are higher. This permits the grains to fracture at lower differential stresses on the aggregate as a whole.

In the experimentally deformed materials, both the twin lamellae in the calcite cement and the fractures in the detrital grains developed concomitantly in response to the same simulated tectonic conditions.

## Summary and Conclusions

The consistent results from experimentally deformed sand crystals and Tensleep and Supai calcite-cemented sandstones indicate that, statistically, both the calcite cement and the detrital grains deform in response to the principal stresses across the boundaries of the specimen as a whole rather than to local stress concentrations at grain contacts. The facts that lead to this conclusion are:

1. The most conspicuous feature of deformed calcite is twin lamellae that develop parallel to $e\{01\bar{1}2\}$.

2. The twin-lamellae spacing index increases with increased strain of the specimen (table 1). This effect is clear when different specimens or differently strained parts of the same specimen are compared (e.g., specimen 911).

3. Resolved shear-stress coefficient data indicate that (*a*) 74 per cent of the best-developed set of lamellae ($e_1$) form with respect to the load on the specimen as a whole, (*b*) the average resolved shear-stress coefficient on $e_1$ lamellae is 0.27, and (*c*) the reliability of correctly identifying $e_1$ lamellae is good in specimens with spacing-index values less than 250. In more highly deformed specimens (e.g., specimen 780) identification of true $e_1$ lamellae is more difficult (table 2).

4. Orientations of principal stresses deduced from $e_1$ lamellae are in good agreement with the known orientations (fig. 16, *a–d*).

5. Strain calculated from rotated lamellae correlates with that measured experimentally (e.g., specimen 877).

6. The majority of microfractures in all specimens are oriented perpendicular to $\sigma_3$; that is, they are extension fractures (figs. 5, 7, and 14).

7. Microscopic and macroscopic shear zones are inclined at approximately 30° to $\sigma_1$ (pls. 2*B*, *c*, and 4).

8. The fracture index increases with increased strain of the specimen (table 1).

9. Orientation and spacing of microfractures tend to be independent of mineralogy, particularly in the sand crystals, where quartz and feldspar grains occur in about equal abundance.

10. The marked relationship between microfractures and principal stresses greatly overshadows the slight tendency for microfractures in quartz grains to parallel *r* and *z*. Accordingly, these microfractures are little affected by crystallographic control.

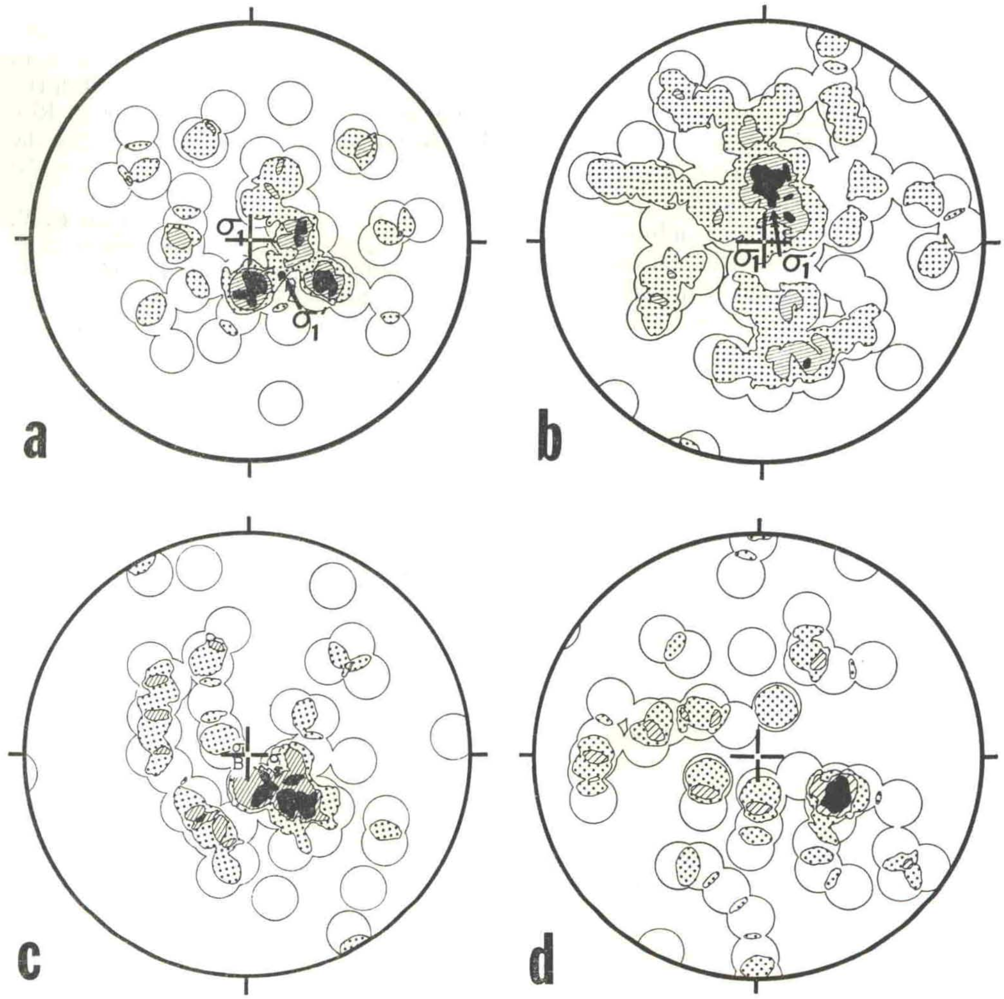


FIG. 16.—Diagrams illustrating orientation of compression axes derived from $e_1$ twin lamellae in specimens 762, 725, 778, and 780. Plane of each diagram is oriented normal to the long axis of the deformed cylinder, and $\sigma_1$ is at the center. *a*, specimen 762. Diagram of 50 compression axes. Contours: 2, 4, 6, and 8 per cent per 1 per cent area; 10 per cent maximum. Center of gravity ($\sigma_1'$) is about 20° SE. of center. *b*, specimen 725. Composite diagram of 100 compression axes. Contours: 1, 2, 4, and 6 per cent per 1 per cent area; 10 per cent maximum. Center of gravity ($\sigma_1'$) is about 10° N. of center. *c*, specimen 778. Diagram of 50 compression axes. Contours: 2, 4, 6, and 8 per cent per 1 per cent area; 10 per cent maximum. Center of gravity ($\sigma_1$) is 10°–15° SE. of center. *d*, specimen 780. Composite diagram of 50 compression axes. Contours: 2, 4, 6, and 8 per cent per 1 per cent area; 12 per cent maximum. There is a general grouping of the axes about the center.

11. The consistent preferred orientation of microfractures relative to the principal stresses indicates that, although stresses may be transmitted through grain contacts, the points of contact do not control the orientation of the fractures observed here.

12. Uniform pressure alone does not produce twinned calcite or fractured detrital grains. When these features are present, tectonism is most probably indicated.

13. In calcite-cemented sandstones both the twin lamellae in the calcite and the fractures in the detrital grains develop concomitantly under the same similated tectonic conditions.

ACKNOWLEDGMENTS.—The writer wishes to thank D. V. Higgs and J. W. Handin, Shell Development Company, and J. J. W. Rogers, Rice University, for their guidance in initiating the study and for their helpful suggestions in the preparation of this paper. In addition, the writer wishes to thank J. W. Handin, R. V. Hager, Jr., and J. N. Feather for experimentally deforming the specimens studied in this investigation and the Shell Development Company for permission to publish this work.

## REFERENCES CITED

ANDERSON, E. M., 1951, The dynamics of faulting and dike formation with applications to Britain: 2d ed., London, Oliver & Boyd, 206 p.

ANDERSON, J. L., 1945, Deformation planes and crystallographic direction in quartz: Geol. Soc. America Bull., v. 56, p. 409–430.

BELL, J. F., 1941, Morphology of mechanical twinning in crystals: Am. Mineralogist, v. 26, p. 247–261.

BLOSS, D. F., 1957, Anisotropy of fracture in quartz: Am. Jour. Sci., v. 255, p. 214–225.

BONHAM, L. C., 1957, Structural petrology of the Pico anticline, Los Angeles County, California: Jour. Sed. Petrology, v. 27, p. 251–264.

BORG, I., FRIEDMAN, M., HANDIN, J., and HIGGS, D. V., 1960, Experimental deformation of St. Peter sand: A study of cataclastic flow: Geol. Soc. America Mem. 79, 382 p.

——— and MAXWELL, J. C., 1956, Interpretation of fabrics of experimentally deformed sands: Am. Jour. Sci., v. 254, p. 71–81.

——— and TURNER, F. J., 1953, Deformation of Yule marble: VI. Identity and significance of deformation lamellae and partings in calcite grains: Geol. Soc. America Bull., v. 64, p. 1343–1362.

BREWSTER, D., 1826, On a new cleavage in calcareous spar with a notice of a method of detecting secondary cleavage in minerals: Edinburgh Jour. Sci., v. 9, No. 18, p. 311–314.

CHAYES, F., 1956, Petrographic modal analysis: An elementary statistical appraisal: New York, John Wiley & Sons, 113 p.

CHRISTIE, J. M., 1958, Dynamic interpretation of the fabric of a dolomite from the Moine thrust zone in north-west Scotland: Am. Jour. Sci., v. 256, p. 159–170.

———, HEARD, H. C., and LAMORI, P. N., 1960, Experimental deformation of quartz single crystals at 27-30kb confining pressure and 24° C.: Geol. Soc. America Bull., v. 71, p. 1842.

COULOMB, M., 1776, Sur une application des règles maximis et minimis à quelques problèmes de statique, relatif à l'architecture: Acad. Sci. Paris Mém. Math. Phys., v. 7, p. 343–382.

CRAMPTON, C. B., 1958, Structural petrology of Cambro-Ordovician limestones of the north-west Highlands of Scotland: Am. Jour. Sci., v. 256, p. 145–158.

FAIRBAIRN, H. W., 1939, Correlation of quartz deformation with its crystal structure: Am. Mineralogist, v. 24, p. 351–368.

GILMOUR, P., and CARMAN, M. F., 1954, Petrofabric analysis of the Lock Tay limestone from Strachur: Argyll, Geol. Mag., v. 91, p. 49–60.

GRIGGS, D. T., 1936, Deformation of rocks under high confining pressure: Jour. Geology, v. 44, p. 541–577.

——— 1939, Creep of rocks: *ibid.*, v. 47, p. 225–251.

——— and BELL, J. F., 1938, Experiments bearing on the orientation of quartz in deformed rocks: Geol. Soc. America Bull., v. 49, p. 1723–1746.

——— and HANDIN, J., 1960, Observations on fracture and a hypothesis of earthquakes: Geol. Soc. America Mem. 79, 382 p.

——— and MILLER, W. B., 1951, Deformation of Yule marble: I. Compression and extension experiments on dry Yule marble at 10,000 atmospheres confining pressure, room temperature: Geol. Soc. America Bull., v. 62, p. 853–862.

———, TURNER, F. J., BORG, I., and SOSOKA, J., 1951, Deformation of Yule marble: IV. Effects at 150° C.: Geol. Soc. America Bull., v. 62, p. 1385–1406.

———, ———, ———, — ——— 1953, Deformation of Yule marble: V. Effects at 300° C.: *ibid.*, v. 64, p. 1327–1342.

———, ———, and HEARD, H., 1960, Deformation of rocks at 500° C. to 800° C.: Geol. Soc. America Mem. 79, 382 p.

HAFNER, W., 1951, Stress distribution and faulting: Geol. Soc. America Bull., v. 62, p. 373–398.

HALL, E. O., 1954, Twinning and diffusionless trans-formations in metals: London, Butterworths Scientific Publishers, 181 p.

HANDIN, J., 1953, An application of high pressure in geophysics: Experimental rock deformation: Am. Soc. Mech. Engineers Trans., v. 75, p. 315–324.

——— and FAIRBAIRN, H. W., 1955, Experimental deformation of Hasmark dolomite: Geol. Soc. America Bull., v. 66, p. 1257–1273.

——— and GRIGGS, D. T., 1951, Deformation of Yule marble: II. Predicted fabric changes: Geol. Soc. America Bull., v. 62, p. 863–886.

——— and HAGER, R. V., JR., 1957, Experimental deformation of sedimentary rocks under confining pressure: Tests at room temperature on dry samples: Am. Assoc. Petroleum Geologists Bull., v. 41, p. 1–50.

——— — ——— 1958, Experimental deformation of sedimentary rocks under confining pressure: II. Tests at high temperature: *ibid.*, v. 42, p. 2892–2934.

HANSEN, E. C., BORG, I. Y., and MAXWELL, J. C., 1959, Dynamic significance of quartz lamellae: Jour. Geophys. Research, v. 64, p. 1104.

HIGGS, D. V., and HANDIN, J., 1959, Experimental deformation of dolomite single crystals: Geol. Soc. America Bull., v. 70, p. 245–278.

HUBBERT, M. K., 1951, The mechanical basis for certain familiar geologic structures: Geol. Soc. America Bull., v. 62, p. 355–372.

——— and RUBEY, W. W., 1959, Role of fluid pressure in mechanics of overthrust faulting, Part I: Geol. Soc. America Bull., v. 70, p. 115–166.

INGERSON, E., and RAMISCH, J. L., 1942, Origin of shapes of quartz sand grains: Am. Mineralogist, v. 27, p. 595–606.

KNOPF, E. B., 1949, Fabric changes in Yule marble after deformation in compression: Am. Jour. Sci., v. 247, p. 537–569.

MCINTYRE, D. B., and TURNER, F. J., 1953, Petrofabric analysis of marbles from Mid-Strathspey and Strathavon: Geol. Mag., v. 90, p. 225–240.

ODÉ, H., 1957, Mechanical analysis of the dike pattern of the Spanish Peaks Area, Colorado: Geol. Soc. America Bull., v. 68, p. 567–576.

PABST, A., 1955, Transformation of indices in twin gliding: Geol. Soc. America Bull., v. 66, p. 897–912.

ROWLAND, R. A., 1946, Grain-shape fabrics of clastic quartz: Geol. Soc. America Bull., v. 57, p. 547–564.

SANFORD, A. R., 1959, Analytical and experimental study of simple geologic structures: Geol. Soc. America Bull., v. 70, p. 19–52.

TURNER, F. J., 1948, Mineralogical and structural evolution of the metamorphic rocks: Geol. Soc. America Mem. 30, 342 p.

——— 1949, Preferred orientation of calcite in Yule marble: Am. Jour. Sci., v. 247, p. 593–621.

——— 1953, Nature and dynamic interpretation of deformation lamellae in calcite of three marbles: *ibid.*, v. 251, p. 276–298.

——— and CH'IH, C. S., 1951, Deformation of Yule marble: III. Observed fabric changes due to deformation at 10,000 atmospheres confining pressure, room temperature, dry: Geol. Soc. America Bull., v. 62, p. 887–906.

———, GRIGGS, D. T., CLARK, R. H., and DIXON, R. H., 1956, Deformation of Yule marble: VII. Development of oriented fabrics at 300° C.–500° C.: Geol. Soc. America Bull., v. 67, p. 1259–1294.

———, ———, and HEARD, H., 1954, Experimental deformation of calcite crystals: Geol. Soc. America Bull., v. 65, p. 883–934.

———, ———, ———, and WEISS, L. E., 1954, Plastic deformation of dolomite rock at 380° C.: Am. Jour. Sci., v. 252, p. 477–488.

WEISS, L. E., 1954, A study of tectonic style—structural investigation of a marble-quartzite complex in southern California: Univ. California, Geol. Sci., v. 30, No. 1, p. 1–102.